ANALYSIS OF THE GEOMETRICAL IMPACT ON THE RUBBER DAMPER PROPERTIES

NG SOO SIEN

UNIVERSITI TUNKU ABDUL RAHMAN

ANALYSIS OF THE GEOMETRICAL IMPACT ON THE RUBBER DAMPER PROPERTIES

NG SOO SIEN

A project report submitted in partial fulfilment of the requirements for the award of Bachelor of Engineering (Honours) Mechanical Engineering

Lee Kong Chian Faculty of Engineering and Science
Universiti Tunku Abdul Rahman

April 2022

DECLARATION

I hereby declare that this project report is based on my original work except for citations and quotations which have been duly acknowledged. I also declare that it has not been previously and concurrently submitted for any other degree or award at UTAR or other institutions.

Signature	:	
Name	:	Ng Soo Sien
ID No.	:	17UEB01889
Date	:	22 April 2022

APPROVAL FOR SUBMISSION

I certify that this project report entitled **"ANALYSIS OF THE GEOMETRICAL IMPACT ON THE RUBBER DAMPER PROPERTIES"** was prepared by **NG SOO SIEN** has met the required standard for submission in partial fulfilment of the requirements for the award of Bachelor of Engineering (Honours) Mechanical Engineering at Universiti Tunku Abdul Rahman.

Approved by,

Signature	:	
Supervisor	:	Ts Dr King Yeong Jin
Date	:	24 April 2022

ACKNOWLEDGEMENTS

I would like to express my thanks to my supervisor, Ts. Dr. King Yeong Jin, for his valuable advices and guidances given to me during this period. It is with his guidances that I know how to carry out my project, particularly on the literature review and methodology planning.

Moreover, I should not forget about my friend who gave me emotional support during the stressful moments of my final year project. He gave me the strength to continue to move forward despite facing seemingly insurmountable problems in my work. Therefore, I would say part of the success in this project is due to him, and I wish him all the best in his final year project as well.

Lastly, I also wanted to express my gratitude to my parents and sibling for giving me comfort during these times. Their support is also what motivates me to overcome the obstacles in my project and successfully carry out the simulation work.

ABSTRACT

Rail pad is a rubber damper used in the railway industry to lessen rail vibration and noise pollution caused by trains moving over the rail. The rail pad is placed between the rail and the sleepers, forming a soft interface between them that isolates vibration. The findings from many authors have demonstrated that the stiffness of rail pad is the critical parameter in determining the dynamic performance of rail track and should be given the utmost attention. Actual rail pads have certain geometrical features, such as studs and grooves, rather than being just a flat piece of rubber. However, there are no studies found in existing literature that are related to the impact of these geometrical features on the dynamic properies of rail pad. Moreover, other geometries can also be proposed on the rail pad, which also requires investigation onto its' impact on rail pad's dynamic properties. Hence, this study investigates the geometrical impact of normal, studded, grooved, holed, cut-out, and shaped rail pad designs onto their dynamic stiffness and energy dissipation by using simulation. In this study, ANSYS Transient Structural was used, and the Prony series material data for FC9 rail pad and dynamic loading conditions were referred from the literature as input for the simulation. From the simulation result, hysteresis loop was obtained and the dynamic properties were computed. The result of this study shows that the thickness is the only feature that can effectively increase dynamic stiffness and decrease energy dissipation, while other features or designs cannot. Moreover, thickness was found to be the most significant feature among all features discussed in this study, with dynamic stiffness improvement ratio (IR) range of 0.835 to 2.376 and energy dissipation IR range of 0.448 to 1.172. The second and third most significant features were also found to be the stud and cut-out features respectively. The dynamic stiffness and energy dissipation IRs for stud feature are in the range of 0.198 to 0.470 (stud diameter) and 1.734 to 3.443 (stud diameter) respectively. As for the cut-out feature, dynamic stiffness and energy dissipation IRs are in the range of 0.580 to 0.927 and 1.032 to 1.369 respectively. In addition, all the features discussed in this study except hole and shape causes a trade-off between dynamic stiffness and energy dissipation as the features are introduced.

TABLE OF CONTENTS

LIST OF TABLES

LIST OF FIGURES

LIST OF SYMBOLS / ABBREVIATIONS

W	strain energy, J
I	strain invariant of left Cauchy-Green deformation tensor
λ	principal stretch ratio
E	elastic modulus, Pa
η	viscosity, Pa.s
τ	relaxation time
k	dynamic stiffness
t	time, s
F	force, N
D	deformation, m

CR	chloroprene rubber
NBR	nitrile rubber
IR	improvement ratio
R^2	coefficient of determination

LIST OF APPENDICES

CHAPTER 1

INTRODUCTION

1.1 General Introduction

Rubber is a soft but highly elastic material. It is capable of sustaining large strain without experiencing plastic deformation or failure before it fully regains its' original shape and size upon removal of the load. Rubber also has intrinsic damping property that allows it to dissipate energy when strained. Due to these properties of rubber, it is used to make rubber damper or isolator to isolate the vibration originated from the vibrating source to protect structures, while also dissipating vibrational energy to lessen the dynamic force created. Some of the examples of rubber damper are rubber bearing, engine mount, and shaft damping ring.

Rubber damper is also widely used in railway to lessen the vibration induced by moving trains that transmits to the structures below the rail, such as the sleeper and ballast. The rubber damper used in railway is called rail pad, and it is placed between the rail and sleeper to serve as soft interface between the two track components. The justification is to prevent the cracking of the concrete sleeper under the rail due to excessive rail vibration (Sol-Sanchez, Moreno-Navarro and Rubio-Gamez, 2015). It is also implemented to minimise the noise produced as a result of uncontrolled vibration of the track. By referring to the works of various authors, the overall track stiffness was demonstrated to be an important parameter that determines the dynamic performance of the track during the passage of train (Chen and Zhou, 2020; Xin et al., 2020; He et al., 2018). Therefore, the rail pads need to have a suitable stiffness that can appropriately attenuate the overall track stiffness to achieve desirable track dynamic response.

Some researches were performed to study the impact of rubber damper geometry on their properties in hopes of optimising rubber damper design. For example, for the rubber damper used in shear-type rail fastening system, it was found that widening the rubber width can reduce the stiffness of the rubber damper significantly, while increasing its' height and inclined angle produce the opposite effect (Ouyang et al., 2015). On the other hand, it was shown that increasing the thickness of for rail pad and pad-like rubber results in lower stiffness (Zakeri et al. 2021; Sol-Sanchez, Moreno-Navarro and Rubio-Gamez, 2014). Studies on rail pads or rubber pads mainly focus on the pad thickness as the main geometrical parameter to alter stiffness. However, rail pads can have certain design features, such as grooves and studs, which could have influenced their stiffness as well. Furthermore, other possible geometrical alterations on rail pads can also be introduced to observe their influence on stiffness, such as changing the overall shape of the rail pads into circle. Hence, more researches are required to understand the impact of geometry on rail pad stiffness.

1.2 Importance of the Study

Rail transport is a favourable transportation mode in many parts of the world due to their large transportation capacity for cargoes and passengers. Not only that, it is also associated with relatively lesser environmental impact and higher efficiency when compared to road transport such as lorries (Sol-Sanchez, Moreno-Navarro and Rubio-Gamez, 2015). Especially due to the widespread construction of high-speed railway in developing countries like China, the railway industry is rapidly expanding and has good future prospect. Simulation studies related to geometry of rail pads are thus needed to facilitate future development of the railway industry. This study will be able to provide insights into the impact of geometry in altering the rail pad properties by using simulation. Especially for grooved and studded rail pads, which are commonly implemented in the real world, this study can improve our current understanding on the influence of these geometrical features on the rail pad properties. In addition, from the simulation result, this study will also be able to identify the significance of the features in contributing to rail pad properties so that material- and cost-optimising design initiatives can be explored in future research.

1.3 Problem Statement

According to a study from Sol-Sanchez, Moreno-Navarro and Rubio-Gamez (2014), different thickness of the rail pad can produce different stiffness, such that increasing the pad thickness will yield a softer pad. Therefore, the rail pad stiffness is typically adjusted to the desired value by changing the thickness. However, rail pads also have other geometrical features that could possibly influence the stiffness. The rail pads usually possess grooves or circular studs on their upper surface instead of being just a plain rubber pad. The contribution of these geometrical features to the rail pad stiffness is not studied in the literature. As a result, these features on rail pads are designed arbitrarily by manufacturers according to experience and not based on any design guidelines. Hence, studies are needed to investigate the influence of these geometrical features on the rail pad properties.

Moreover, other geometry alteration can be done on rail pads as well. Some examples are cutting out holes from the rail pads in order to save material and cost or changing the overall shape of rail pads from square to circle. Similarly, the effects of these geometrical changes on rail pad properties are not studied in the literature. The geometrical features that can significantly impact the properties are also not identified. Therefore, studies also need to be conducted to identify other possible geometrical changes and also their significance in affecting the properties.

1.4 Aim and Objectives

This study aims to investigate the impact of different geometrical features or alterations, such as grooves, studs, and cut-outs, on the rail pad's dynamic stiffness and energy dissipation under loading condition similar to the passage of train. The objectives of the study are as follow:

(i) To propose various rail pad designs with different dimensions and geometrical features.

(ii) To evaluate the influence of different geometry on the rail pad's dynamic stiffness and energy dissipation using simulation.

(iii) To evaluate the significance of the influence of each geometrical feature in affecting rail pad dynamic stiffness and energy dissipation.

1.5 Scope and Limitation of the Study

There are many kinds of rubber damper created for different applications, so the scope of this study focused on rail pad only, which is a type of rubber damper used in railways to abate excessive vibration of the track. With conclusion from numerous studies that the track stiffness is the crucial parameter to achieve desirable dynamic performance, the properties of rail pad that was investigated in this study is the dynamic stiffness. Aside from that, since most rail pad studies only focused on stiffness, the energy dissipation of the rail pad was also investigated as an additional finding of this study. In short, this study investigated the impact of numerous geometrical features on the rail pad dynamic stiffness and energy dissipation using simulation.

One of the limitations in this study is limited rail pad material. Rail pads can be made of many materials; however, only cork rubber, which is the material for FC9 rail pads, is considered in this study due to limited sources providing the material data of the rail pads. Thus, the result of this study might not be accurate for rail pad of other material. Another limitation is the simulation setup. Simulation studies done on railway usually use the vehicle-track coupled dynamic model to simulate the passage of train over the rail to study track vibration. However, in this study, a sinusoidal load was applied on the rail pads instead for simplicity which might sacrifice some accuracy on the result.

1.6 Contribution of the Study

The properties of rail pad, especially dynamic stiffness, is crucial to the dynamic performance of the rail. The stiffness should not be too small in order to preserve the lifespan of rail fasteners and reduce amplitude of rail vibration (Shi et al., 2017). It should also not be too high as to cause severe rail vibration and noise. Therefore, the dynamic properties of rail pad need to be suitably adjusted for optimal performance in the railway. The adjustments on the dynamic properties are usually done by altering the geometry of the rail pad. Thus, this study demonstrates via simulation the impact of the different rail pad designs and features on the rail pad's dynamic properties, such as the trend of the properties when a certain feature is adjusted. Moreover, from the simulation result, the significance of the features in influencing dynamic properties is also determined in this study to pinpoint the features that require the most attention for attenuating dynamic properties. Not only that, this study also explores rail pad designs that aim at reducing material and cost so as to inspire future researches in cost-effective design. Finally, the simulation result of this study also serves as a reference in setting the direction of future work in studying the geometrical impact on rail pad's properties.

1.7 Outline of the Report

This report is divided into five (5) chapters, which includes the introduction of the study, review of existing literature, work flow and methods, discussions of results, and conclusions and recommendations.

Chapter 1 is the introduction, and it begins with a general introduction on the topic of this study: rail pad. The general introduction briefly discusses on the basic knowledge of the topic to provide a brief understanding of this study. This chapter is then followed by explaining on the problem and importance of this study, while also outlining the objectives. The scope and limitation as well as the contribution of the study is also discussed in this chapter.

Chapter 2 is the literature review. This chapter discusses thoroughly on the properties of rubber and its' application in rubber damper. In addition, the various constitutive models for modelling rubber behaviour are also discussed here. After that, it is followed by an in-depth discussion on the rail pad, rail track, and relevant knowledge on rail pad stiffness. This chapter then ends by reviewing the literature related to the effect of geometry on the rubber damper.

Chapter 3 is the methodology and work plan. This chapter outlines the detail procedure carried out in this study. This includes the obtaining of the rubber material data from the literature and also the assumptions in constructing the dynamic loading function for simulation. Moreover, the rail pad geometries considered, simulation setup, and result calculations are also outlined.

Chapter 4 is the results and discussions. It discusses on the result obtained from simulation and interprets the result. This chapter has seven (7) sections, corresponding to each rail pad design plus an overview for all the rail pad designs. The discussion for each design includes the trend of the dynamic properties when certain feature is altered and the significant features that influences the properties. This chapter then ends with an overall discussion on the results of all the rail pad designs.

Chapter 5 is the conclusion and recommendations. It concludes the results and findings in this study. Moreover, recommendations are also provided for future research work to develop the field of knowledge in the literature.

CHAPTER 2

LITERATURE REVIEW

2.1 Introduction

The literature review section first begins with a general introduction to the rubber material which covers the rubber properties, vulcanisation process, and rubber types. The next section discusses on the constitutive models of rubber used for modelling their stress-strain behaviour. This section is divided into two subsections: hyper-elastic model and viscoelastic model. Both types of models are used depending on the loading condition. Moving on, the next section is on the rubber damper application which explores the engineering applications of rubber damper in the real world. The section followed by is then a comprehensive discussion on the focus of this study, that is rail pads. This section consists of five subsections. The first subsection generally introduces the railway industry and the necessity of rail pads. The second subsection explains the components in the track and also the types of tracks available in the world. Next, the third subsection reviews on studies relating to the significance of rail pad stiffness in rail track. The fourth subsection then further explains on the factors that affects the rail pad stiffness. Lastly, the final subsection reviews studies on the impact of geometry on the properties of rubber damper and rail pads. Finally, the literature review ends with a short summary before moving to the next chapter.

2.2 Rubber Material

Rubber, also known as elastomer, is a type of amorphous polymer characterised by its' excellent elastic property that allows itself to completely recover the deformation imposed after subjected to large straining or stretching. Its' elastic nature can be attributed to the long molecular chains that are crosslinked, kinked, and convoluted inside the material (Callister and Rethwisch, 2014). When load is applied onto the rubber, these chains unfold and straighten in response. Once the load is removed, the straightened chains spring back into their original conformations and restore the macroscopic shape and dimensions of the material (Callister and Rethwisch, 2014). Aside from that, rubber also displays intrinsic damping capability which provides rubber the ability to dissipate energy when strained. This is due to a portion of the energy supplied to deform the rubber is directed to counteract resistance to the molecular chain's motion when the molecular structure is broken (Kareaga Laka, 2016).

Rubber in its' crude form is not usable as it is sticky and cannot support any loads. Thus, it has to undergo vulcanisation process to make it more durable and resilient before applicable to engineering applications. The vulcanisation process is carried out at the cure activation temperature usually around 120 °C – 200 °C, while introducing various compounds such as sulphur compounds and activators into the unvulcanised rubber (Kareaga Laka, 2016). Sulphur atoms from the compounds will serve to bond the polymer backbones together and crosslink the chains in the process, making the rubber harder and stronger (Callister and Rethwisch, 2014).

Rubber can be categorised according to their sources: natural and synthetic. The natural rubber is produced from the latex collected from rubber tree. There is only one type of natural rubber, and its' chemical composition is polyisoprene. On the other hand, synthetic rubber is derived artificially from by-products of petroleum. Unlike natural rubber, synthetic rubber consists of many kinds, each with different chemical make-ups. Some of the common synthetic rubbers used in engineering are chloroprene rubber (CR) and nitrile rubber (NBR).

2.3 Constitutive Models of Rubber

In order to model rubber behaviour, constitutive models need to be used to represent the rubber behaviour. There are two (2) categories of rubber model, which is the hyper-elastic model and the viscoelastic model. Both models are used for different scenarios of loadings on rubber, and each of them has its' own characteristics. The different available models for both categories are presented in this section.

2.3.1 Hyper-elastic Model

Due to the incredible elasticity of rubber, it is considered as a hyper-elastic material. The characteristic of the stress-strain behaviour of rubber is that it is highly non-linear. Due to that, Hooke's law is not applicable to predict rubber response unless the stress and deformation in concern are small. Therefore, many phenomenological hyper-elastic models were developed by researchers to model the non-linear stress-strain behaviour of rubber. Many models have one assumption in common, that is the rubber's stress and strain states can be described by the strain energy density function alone as suggested by Mooney (1940). Hence, the hyper-elastic models are usually expressed in terms of strain energy, W of the deformed material in relation to other strain-related variables, such as principal stretch ratios or strain invariants.

2.3.1.1 Generalised Mooney Rivlin Model

One of the most famous and commonly used hyper-elastic model is the Mooney-Rivlin model. It was developed by Mooney (1940), and was expressed in the typically seen strain invariant form by Rivlin (1948). It was proposed under the assumptions that rubber is isometric or incompressible while deforming, isotropic in the plane normal to the stretch direction after the rubber is deformed, and isotropic prior to any deformation (Mooney, 1940). The generalised Mooney-Rivlin model is expressed in the following way:

$$W = \sum_{i=0,j=0}^{N} C_{ij}(I_1 - 3)^i (I_2 - 3)^j \tag{2.1}$$

where C_{ij} is material constant determined from experiment. I_1 and I_2 referred to the first and second invariants taken from the left Cauchy-Green deformation tensor. The order, N used depends on the number of inflection points in the stress-strain curve but usually does not go beyond third order as the model then becomes increasingly complex. Based on the order, the model will require different number of parameters to establish; for first-, second-, and third-order, the number of material constants is two, five, and nine respectively. The Mooney Rivlin model is generally applicable for many situations. It is suitable to model rubber behaviour from low to moderate deformation; however, it becomes inaccurate when deformation is large (Li et al., 2020).

2.3.1.2 Yeoh Model

On the basis of the strain energy density function assumption, the Yeoh model was proposed, taking the form of a cubic strain energy function. It is capable of capturing the variation in shear modulus with increasing strain, which is an added strength when compared to Mooney-Rivlin model (Yeoh, 1993). As a result, it can accurately describe a wider range of deformation and applicable for large strain application (Li et al., 2020). The Yeoh model expression considering rubber incompressibility is as followed:

$$W = \sum_{i=1}^{3} C_{i0}(I_1 - 3)^i = C_1(I_1 - 3) + C_2(I_1 - 3)^2 + C_3(I_1 - 3)^3 \quad (2.2)$$

C_{i0} is material constant, while I_1 is the same as explained above. The model is sometimes preferred in studies due to its' simplicity over other hyper-elastic models as it is a function only of the first invariant unlike the Mooney-Rivlin model, which is a function of both first and second invariants (Habieb, Valente and Milani, 2019).

2.3.1.3 Ogden Model

Ogden model is the most commonly used model, especially for analysing the behaviour of small rubber parts like seals and O-rings (Kim et al. 2012). One major benefit of this model is that test data can be directly implemented as it is expressed in terms of stretch ratios rather that strain invariants. Moreover, Ogden model can also show very close agreement with experimental data in large strain scenarios, and it is generally more flexible in fitting the rubber curve due to the fact that stretch ratio exponents, α_i are real number instead of integer such as those in Mooney-Rivlin model (Kim et al., 2012). The Ogden model can be written in the following form:

$$W = \sum_{i=1}^{N} \frac{\mu_i}{\alpha_i}\left(\lambda_1^{\alpha_i} + \lambda_2^{\alpha_i} + \lambda_3^{\alpha_i} - 3\right) \quad (2.3)$$

where λ_1, λ_2, and λ_3 represents the principal stretch ratios. μ_i and α_i are empirical constants determined from experiment. Usually, third order Ogden model ($N = 3$) is sufficiently accurate to model rubber behaviour for most engineering application.

2.3.2 Viscoelastic Model

Hyper-elastic models are used to describe the static response of rubber and only applicable to static loading scenarios or when quasi-static assumption is made. When dynamic loads originating from a vibration source is acting on the rubber, its' behaviour can no longer be described by hyper-elastic models alone. Instead, the stress-strain response now exhibits viscoelasticity, and thus the viscoelastic models are required. Viscoelastic models are able to characterise the dynamic characteristics of rubber, which include the dynamic stiffness and damping, by considering also time or frequency as factors that influence the rubber response. The models have an elastic component capturing the elastic stress caused by strain, and also a viscous component describing the viscous stress induced by rate of deformation.

2.3.2.1 Maxwell Model and Kelvin-Voigt Model

The simplest model used to capture viscoelasticity is the Maxwell and Kelvin-Voigt models. The Kelvin-Voigt model reconstructs viscoelasticity by replacing the rubber material with a parallelly connected spring and dashpot elements with a respective elastic modulus, E and viscosity, η. On the other hand, Maxwell model models viscoelasticity by connecting the spring and dashpot elements in series. Both models have their respective strengths in modelling viscoelasticity. Kelvin-Voigt model is suitable for evaluating creep effect, while Maxwell model is appropriate for studying the material response during stress relaxation (Fatima, Shafi and Anjum, 2019). Although not explicitly mentioned in the studies, the Kelvin-Voigt model is commonly used as a simple model for rail pads when railway-track interaction is studied (Bhardawaj, Sharma and Sharma, 2019). However, both models share the same downside of assuming a constant damping and stiffness coefficients, which does not represent the actual rubber properties that are dependent on frequency and amplitude unless its' service condition is well understood, and the dynamic properties used are accurate for that condition.

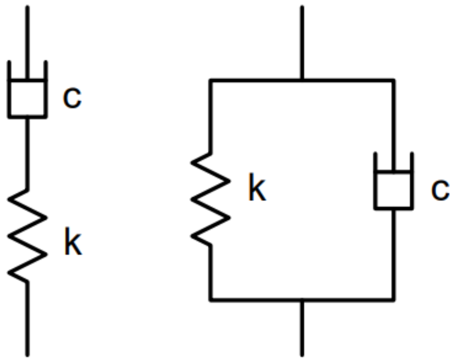

Figure 2.1: Maxwell Model and Kelvin-Voigt Model

2.3.2.2 Generalised Maxwell Model and Prony Series

In order to increase the accurateness of the viscoelastic model, the Generalised Maxwell model can be used instead of the simpler Kelvin-Voigt model or Maxwell model. The Generalised Maxwell model is constructed by arranging many Maxwell models in parallel. The number of parallel branches, N can be set so as to be necessary in capturing the full viscoelastic response of the rubber. Since each Maxwell branches has respectively an elastic modulus, E_i and a viscosity, η_i, the model is able to capture multiple elastic moduli and relaxation times of the rubber. By having more branches, it will then be able to describe the rubber's viscoelastic response in a range of loading frequency, therefore allowing it to characterise the frequency-dependent dynamic properties of rubber (Oregui et al., 2017). Most of the time, the model is modified by connecting an additional spring element in parallel to become the Maxwell-Wiechert model as illustrated in Figure 2.2. Maxwell-Wiechert model can be written mathematically in the form of Prony Series that is typically implemented into finite element software. The relaxation modulus as represented in Maxwell-Wiechert model can be expressed in Prony series (Oregui et al. 2017):

$$E(t) = E_\infty + \sum_{i=1}^{N} E_i \, e^{-\frac{t}{\tau_i}} \tag{2.4}$$

Where E_∞ is the long term modulus of rubber. N refers to the number of parallel branches. E_i and τ_i are the elastic modulus and relaxation time for the i-th branch.

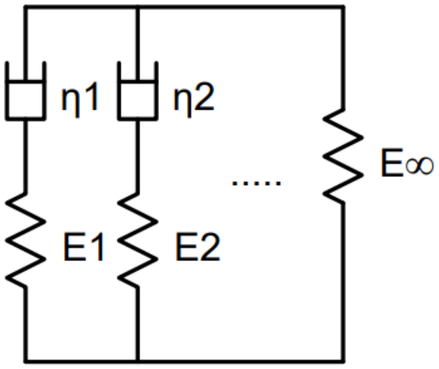

Figure 2.2: Maxwell-Wiechert Model

2.4 Rubber Damper Application

Due to their inherent qualities of low stiffness, energy-dissipating, and excellent elasticity, rubber is widely implemented as vibration damper or isolator that serves to dissipate vibrational energy or to isolate vulnerable objects from vibrating sources. Rubber damper application is very broad as different dampers are designed to cater for different situations, from small rubber absorbers in machinery to huge rubber bearings for protecting civil structures.

Perhaps an important application is to achieve seismic isolation of civil structures by using rubber bearings. Rubber bearings are used to isolate buildings from the ground vibration resulted during an earthquake so as to protect them from collapse. Rubber bearings are designed to possess high vertical stiffness to support the massive weight of the building, while also low lateral stiffness to allow the building to shake in the lateral direction rigidly during the earthquake. With the rubber bearing, the natural period of the building is shifted to a higher period that is typically longer than the usual vibrational period of earthquake in order to avoid the resonance phenomenon (Doshin Rubber, n.d.). The simplest of all rubber bearings is the laminated rubber bearing that has thin rubber layers interspersed with steel shims. The rubber layers provide lateral flexibility, while the steel layers impart vertical stiffness to the bearing (Rahnavard, Craveiro and Napolitano, 2020). Another variant of rubber bearing is the high-damping rubber bearing (HDRB). In this design, the rubber layers are made from high-damping rubber which gives it intrinsic damping quality to eliminate the needs of auxiliary dampers, such as the U-damper made with shaped memory alloy (Doshin Rubber, n.d.). Furthermore, a lead core can be inserted into the centre of the bearing to produce a lead rubber bearing (LRB). The lead core serves a similar function as the high-damping rubber in HDRB. In the event of an earthquake, the lead core deforms plastically as the LRB is laterally sheared due to ground motion, enabling it to dissipate energy transferred to the building to reduce the structural forces occurred in the building's structure.

Another application of rubber isolator is to isolate vibrating machinery or equipment. An example of such rubber isolator is the rubber engine mount. The purpose of the rubber mount is to reduce the adverse, collective effect of vibration caused by the unbalanced reciprocation of engine parts, varying gas pressure, and shaking force in order to maintain passenger comfort and driving stability (Santhosh et al., 2020). Engine mounts are also critical in reducing the noise and vibration harshness (NVH) of automobiles. The mount needs to have high static stiffness to support the engine, while having low dynamic stiffness and damping to achieve good vibration isolation (Santhosh et al., 2020). Aside from that, rubber isolator can also be ring-shaped for applications involving rotating part. An example would be the shaft damping ring used in the helicopter tail drive system. The damping ring is meant to mitigate the excessive bending vibration transmitted to the helicopter body when the system is running at high velocity (Li et al., 2020). In this case, the inner and outer diameters are important dimensions to consider when designing the damping ring as they affect the dynamic stiffness and loss factor significantly (Li et al., 2020).

In addition, rubber is also used to reduce torsional vibration induced on joints. An example of such rubber isolator is the Assembled Rubber Metal Isolator (ARMI) that employs the concept of Neidhart spring (Wu et al., 2020). The ARMI is constructed of an outer metal shell and inner square metal tube; flexible rubber rods are inserted into the four corners between the shell and tube, serving as flexible interface so that the tube can rotate relative to the shell (Wu et al., 2020). The outer shell and inner tube are connected with bolts and nuts to different parts of a machine structure. Vibration coming from sources such as a motor that transmits to the inner tube will thus be dampened before the vibration propagates to the outer shell.

2.5 Rail Pads

The rail pad is a rubber damper used in the railway industry for solving vibration issues. Since rail pads are the rubber damper that will be investigated in this study, this section is dedicated to discuss on the relevant knowledge and background related to rail pad. There are five (5) subsections in this section, that is the railways, rail track, rail pad stiffness, factors affecting rail pad stiffness, and effect of geometry of rubber damper.

2.5.1 Railways

Rail transport refers to the transferring of merchandises, goods, or passengers from one location to another by wheeled vehicle called trains that travel on prebuilt railroads. This mode of transportation is advantageous when compared to road transport, where cargoes or people are transported to their destinations on conventional roadways built for cars, motor vehicles, or lorries, due to their high freight capacity, high efficiency, and also minimal impact to environment (Sol-Sanchez, Moreno-Navarro and Rubio-Gamez, 2015). The rolling stocks (rail vehicle) travel on a pair of rails constructed with steel I-beam that will guide and support the train as it drives forward on the track. When the train travels, the train weight imposes a cyclic, dynamic loading onto the rail section directly below the train wheels, creating vibration of the track and production of noise. Excessive track vibration can lead to the cracking of concrete sleepers that underlies the rails, resulting in frequent and costly railway maintenance (Sol-Sanchez, Moreno-Navarro and Rubio-Gamez, 2015). Significant noise production will also become a nuisance to humans, degrading the quality of life for residents nearby. As a result, rubber rail pads are introduced as rubber damper for the track. The main purpose of rail pads is to isolate and damp the vibration incurred by moving train on the superstructure and substructure below the rail. Other than that, rail pads also serve as electrical insulation between the track rails (Sol-Sanchez, Moreno-Navarro and Rubio-Gamez, 2015).

2.5.2 Rail Track

In order to install the rail, a rail fastening system is necessary to fasten the rail onto the sleepers. The rail fastening system includes rail clips that exert clamping force onto the rail foot to fasten the rail against the sleeper. The rail pad is placed below the rail so that it creates a soft layer between the rail and sleeper that attenuates vibration. There are mainly two types of tracks: ballasted track and slab track (also called ballastless or non-ballasted track).

The rails, fastening system, rail pads, and sleepers form the superstructure in ballasted track. Below the superstructure, there exist a multi-layered substructure made from granular materials which forms the foundation of the track and consists of the ballast, sub-ballast, and subgrade layers. The ballast layer is made from free-draining, coarse granular material that underlies the sleeper and transfers dynamic loads originated from the train to the sub-ballast and subgrade below (Indraratna, Ngo and Rujikiatkamjorn, 2017).

As for the slab track, a flat concrete slab is built to support the rail instead of a ballast layer. The sleepers are cast into the concrete slab. Below the slab is the cement asphalt mortar (CAM) and concrete supporting layers. The slab track is widely used as an alternative to ballasted track for its' better track stability, lesser maintenance, and high durability (Xu, Liu and Yu, 2022). To effectively mitigate vibration issues, a floating slab track is sometimes built where the slab is supported with rubber bearings or steel springs to isolate the slab from the underlying layers (Jin, Zhou and Liu, 2017). Furthermore, isolation layer laid with rubber pad can also be added between the CAM and supporting layers to adapt better to highspeed and heavy freight applications (He et al., 2018).

2.5.3 Rail Pad Stiffness

The most important parameter for railway track is its' overall stiffness as demonstrated by numerous studies. It was shown that overall displacement amplitude of non-ballasted track is influenced by the rail fastener stiffness and elastic modulus of the substructure; higher substructure elastic modulus generally results in smaller vibrational displacement of the rail, embankment, and subgrade layer (Chen and Zhou, 2020). Also, the stiffness gradient at the transition zone between the fixed and floating slab tracks is critical in determining the contact force generated between the train wheels and the rail; As compared to an abrupt jump in track stiffness, a gradual change across the transition zone is more favourable in alleviating the train wheel impact on the rails (Xin et al., 2020). Furthermore, the addition of rubber pad between the supporting layer and concrete slab of slab track was found to significantly mitigate vibration transferred to the supporting layer because the softer pad stiffness dominates the total vertical stiffness of slab track (He et al., 2018). Evidently, these authors show that the vertical stiffness of track determines the dynamic response of the track components. The rail pad thus needs to have the appropriate stiffness to attenuate the track stiffness to achieve desirable track response and reduced vibration.

Usually, the rail pad stiffness should not be too high. This was confirmed by Grassie and Cox (1984) that stiffness of rail pads affects the dynamic reaction during sleeper resonance where stiff pads increase the wheel/rail contact force and surface strain on sleepers. It was also found by Ju, Kuo and Ni (2018) that soft rail pads allow improved slab vibration isolation when the pad’s damping is high; however, stiff rail pads cause vibration isolation to be independent of the damping, and vibration isolation effectiveness is severely limited. Moreover, study conducted in Metro Bilbao has observed that growth of rail corrugation corresponds to wavelength of 80-100 mm was significantly reduced or eliminated by the replacement of stiff rail pads (90 MN/m) with soft ones (60 MN/m), while mean amplitude of the rail profile also saw a 55% reduction after the rail pad replacement (Egana, Vinolas and Seco, 2006).

Nevertheless, when stiff rail pads are used, it is capable of reducing vertical rail displacement considerably, which can preserve the longevity of rail fasteners and improve connection between the rail and structure below (Shi et al., 2017). This is because the enhanced stiffness of the fastening system, that is dominated mainly by rail pad stiffness, restricts the movement of the rail during vibration by maintaining tight connection between rail and sleeper (Chen and Zhou, 2020). Furthermore, stiff rail pads can lessen the rail displacement of poorly supported sleeper as a result of ballast settlement. It was found that changing the pad stiffness from 60 MN/m to 240 MN/m reduces the rail displacement for partially- and un-supported sleepers by 1% – 6% and 2% – 13%

respectively (Zakeri et al., 2020). Hence, the stiffness of rail pads is an important parameter that needs to be well tuned to suit the application of railways in different situation so that the impact of vibration and noise arise from track components and track life preservation is optimally balanced.

2.5.4 Factors Affecting Rail Pad Stiffness

The rail pads are crucial in reducing railway maintenance and ensure durability of the track system. Unfortunately, the rail pad stiffness varies with the service condition during the passage of train, making it difficult to predict in advance the dynamic stiffness of rail pad in play during service. Based on existing studies, temperature is a prominent factor that will alter the stiffness of rail pad. Wei et al. (2016) carried out experimentation on the temperature effect on rail pad stiffness of CR, TPE, and EPDM rail pads. They found the static stiffness for the three rail pads is clearly non-linear with temperature changes. Their stiffness drops greatly with temperature in low temperature range (-40 – 20 °C) but is relatively stable in high temperature range (20 – 70 °C) with the exception of TPE pad which exhibits an abrupt jump in stiffness at 60°C. The findings indicated that it is particularly problematic for railroad in seasonal countries when winter approaches as the rubber becomes too stiff for effective vibration isolation.

Besides that, frequency is also found to be a factor that influences the rail pad stiffness. Depending on the types of train, they travel at different speed on the rail track. Consequently, the frequency at which the train weight imposes on the rail pad will change with train speed. Wei et al. (2017) study the dependency of rail pad’s dynamic properties on temperature and frequency for rail pads used in various fastening systems. They found that both storage modulus and loss factor of rail pad increase gradually with the dynamic load frequency. Besides, they also seen that the storage modulus shares similar trend of temperature dependency of rail pad stiffness as observed in Wei et al. (2016). The loss factor of rail pad was also found to rise with temperature when the temperature is low until it peaks at the glass transition temperature of rubber before dropping with temperature.

Not only that, the dynamic loading amplitude is also a factor that can change rail pad stiffness. The load exerted by the train wheels on the rail corresponds closely to the train weight and is known as the axle load. The axle load is the amplitude of the oscillating load experienced by the rail pads. Wei, Zhang and Wang (2016) have studied on the influence of dynamic amplitude on the rail pad stiffness and found that increasing load amplitude can result in stiffening of the rail pad. They further concluded that the stiffness that considers amplitude and frequency dependencies is more suitable to predict pad stiffness in railway compared to secant stiffness or frequency-dependent (only) stiffness as both representation of stiffness underestimate random vibration levels at high frequency range of 65 – 150 Hz. During service, there is also constant clamping force exerted by the rail fasteners on the rail pads. The force is referred to as the toe load and translates to static preloading on the rail pad. According to Kaewunruen and Remennikov (2008), the dynamic stiffness of studded rubber rail pad was found to increase with the preload level. Its' dynamic stiffness initially increases substantially at low preload level but the stiffness increment becomes lesser as preload increases further.

Finally, Sainz-Aja et al. (2020) have done thorough investigation into all the factors previously mentioned (temperature, toe load, axle load, and frequency) on EPDM, TPE, and EVA rail pads. Their findings basically agree with those discussed above, that is the rail pad stiffness generally increases when temperature reduces, axle load or toe load increases, or excitation frequency increases. They also concluded that the influence of temperature and toe load have higher impact in changing the pad stiffness than axle load and frequency; however, this is not to say that axle load and frequency are insignificant factors.

To summarise the literature discussed above, the rail pad stiffness is altered by the environmental temperature of the railway, axle load resulted from different train load, toe load due to clamping force from rail fasteners, and the dynamic frequency caused by different train speed. These factors are actually due to the intrinsic characteristics of rubber capable of being influenced by temperature, dynamic load frequency and amplitude, and preloading. Therefore, these factors are actually relevant to all rubber dampers and not just exclusively to rail pads.

2.5.5 Effect of Geometry on Rubber Damper

It is widely acknowledged that the geometry of rubber damper or isolator affects their dynamic performance during vibration. Hence, studies have been carried out to study the impact of different geometry alteration to rubber damper properties in order to gain insight into ways of optimising existing rubber damper design. An example of geometrical impact on rubber isolator was demonstrated by Li et al. (2011) who introduced 14 holes into the rubber material of an equipment rubber isolator used for isolating machineries on ships. The introduction of hole feature into the isolator has proven with simulation to reduce the resonant vibration amplitude of the steel plane (floor) by 3.4 dB under excitation force of 10 N when compared to that without holes. Ali, Farhan and Moosa (2017) has also studied the shape factor of anti-vibration rubber to understand the impact of different rubber shape on their operational period by using simulation. It was found that the rubber with hexagon shape produces the lowest deformation and stress intensity as compared to trapezoidal and cylindrical shapes during static and dynamic loadings, concluding that the hexagonal shape is the most suitable among the three shapes for extending operational period of the rubber damper.

The geometrical impact for rubber damper applied in railway is studied as well. Research by Ouyang, Luo and Liu (2015) investigated the various geometrical parameters, including the height, width, and inclined angle, of the rubber absorber used in shear-type rail fastening system (Cologne Egg) to isolate vibration caused by moving train by using finite element analysis. Simulation showed that the vertical stiffness of the rubber is soften prominently by the thickening of rubber width as large width allows free surface to grow during shearing deformation caused by excitation. On the other hand, the increase of rubber height and inclined angle is found to increase the vertical stiffness of the fastening system.

As for rail pad and rubber sheet, it was shown that their thickness is a major factor in affecting the rubber damper stiffness. Zakeri et al. (2021) proposed to place a rubber sheet in the soil bed of machine foundation to achieve better dynamic response during machine vibration and investigated the influence of rubber sheet thickness in improving the dynamic performance. By applying a 6 mm rubber sheet and increasing the thickness up to 24 mm, the foundation's resonant frequency and equivalent shear modulus decreased by 22% and 36% respectively, indicating that increased sheet thickness lowers the dynamic stiffness of the rubber sheet so that it alters the total stiffness of the soil bed. Moreover, Sol-Sanchez, Moreno-Navarro and Rubio-Gamez (2014) examined the effect of thickness on the stiffnesses of rail pads made from recycled deconstructed tires. They discovered that both rail pad stiffnesses increase with reducing thickness, where the stiffnesses rise even more significantly for rail pads with thickness smaller than 6 mm. Furthermore, it was realised that the relation between both the stiffnesses and thickness can be related by a power law model.

Thickness is not the only geometrical parameter of rail pads that can be investigated for their impact on rail pad dynamic properties. In fact, rail pads come with other features, such as grooves cutting into the pad or circular studs protruding from the pad surface. These rail pad designs are not uncommon and are widely used around the world. However, the influence of said features on rail pad properties receive very little attention in the literature as they only focused on the thickness as the main parameter for adjusting the properties, as shown by Sol-Sanchez, Moreno-Navarro and Rubio-Gamez (2014). Similarly, there is no study that investigates possible features aside from grooves and studs that can be introduced into the rail pad design to optimise it.

2.6 Summary

The literature review has included discussion on the basic knowledge of rubber. Because of their intrinsic non-linear stress-strain behaviour and also viscous damping effect, different hyper-elastic and viscoelastic constitutive models are developed to describe their behaviour. With these properties, rubber is then applied in many rubber damper applications. One such application is the rail pads used in railway for reducing excessive track vibration. Various studies have indirectly shown that the important property of rail pads is its' stiffness so that it is capable of attenuating the overall track stiffness to produce desirable track dynamic response. Accordingly, research was carried out to study the impact of geometry on the rail pad stiffness. However, attentions were focused on the thickness of rail pads as the main factor in changing the rail pad properties, which has left out other geometrical features such as grooves and studs. Also, no studies have been done to investigate other geometrical features that can possibly be added to rail pads to influence its’ properties.

Hence, this study is dedicated to understand the influence of various geometrical features on the dynamic properties of rail pads by simulation. The impact of grooves and studs on the rail pad properties that was neglected in previous study will be examined. In addition, other features such as cut-outs will be proposed and introduced to rail pads to further investigate the impact of more geometrical features. From the result of the study, the significance of each feature in influencing the dynamic properties will also be obtained as well. Hence, this study will serve to explore area not studied in previous research.

CHAPTER 3

METHODOLOGY AND WORK PLAN

3.1 Introduction

The work in this study aims to investigate the geometrical impact of different features on the dynamic stiffness and energy dissipation of rail pad. This study is conducted with simulation software in order to simulate the dynamic and static loadings on the rail pad that resembles the passage of train. The dynamic stiffness, energy dissipation, and relevant result data are then calculated and compared. This chapter has six (6) subsections. The first subsection details the material model and data of the rubber used in this study. The second subsection then explains on the loading condition used in simulating the response of rail pad with different geometry. Next, the third subsection is about the designs and features of the rail pads that were proposed and investigated. Afterwards, the fourth subsection explains the setup of the simulation in the software. The fifth subsection then presents about the calculations involved in obtaining the result of this study. Finally, a summary is provided at the end of this chapter.

3.2 Rubber Material Model and Data

As mentioned earlier in the literature review, there are two kinds of constitutive models for rubber, that is hyper-elastic and viscoelastic models. Since the train is a moving weight moving above the rail, the load experienced by the rail pads is dynamic. Therefore, Prony series was chosen to model the rubber behaviour of the rail pad. The relaxation times and stiffnesses for the Prony series is referred from Oregui et al. (2017). The source has provided the material data for FC9 rail pad that is made from cork rubber for multiple degrees of preload and temperature conditions, which is 0 kN, 6 kN, 12 kN, and 18 kN; and 0 °C, 10 °C, and 23 °C respectively. The preload amount used in this study is 18 kN as Sainz-Aja et al. (2020) suggested it to be the standard value. The temperature is chosen to be as close as possible to the temperature in Malaysia, which is 23 °C. Hence, the selected Prony series material data from the source was tabulated in Table 3.1.

Table 3.1: Prony Series Material Data for Cork Rubber

Relaxation Time		Stiffness	
Parameter	Relaxation Time (s)	Parameter	Stiffness at 18 kN Clamping Force, 23°C (MPa)
N/A	N/A	E_∞	133
τ_1	0.1	E_1	63
τ_2	0.01	E_2	50
τ_3	0.001	E_3	80
τ_4	0.0001	E_4	41

3.3 Loading Condition

The loads on the rail pad consist of two components: dynamic and static loads. The dynamic load is caused by the passage of train over the rail. The load is sinusoidal and oscillates between the value of zero and twice the dynamic amplitude. The dynamic amplitude on the rail pad is taken to be 31.5 kN, which is one of the stated amplitude values stipulated in EN 13481-2 and EN 13146-9 of the European Standards as mentioned in Sainz-Aja et al. (2020). Also, a high-speed train with maximum speed up to 350 km/h is assumed to travel over the rail in this study. By assuming an 18 m distance between the train bogies, the corresponding frequency produced by the train is 5 Hz (Sainz-Aja et al., 2020). Meanwhile, the static load is a result of the clamping force exerted by the rail fasteners. It is set to be 18 kN as stated before. By the superposition of the loads, the time function of the total load imposed on the rail pad is expressed as follow:

$$\begin{aligned} Load\ (kN) &= Dynamic\ Load\ (kN) + Static\ Load\ (kN) \\ &= (31.5\, sin(2\pi \times 5 \times t) + 31.5) + (18) \\ Load\ (kN) &= 31.5\, sin(10\pi t) + 49.5 \end{aligned} \tag{3.1}$$

where t is the time variable.

3.4 Rail Pad Geometry

The dimension of FC9 rail pads is 152 mm × 152 mm × 4.5 mm (Oregui et al., 2016). However, the geometries on rail pads were developed by using the same rail pad dimensions but with thickness of 10.5 mm as baseline design (152 mm × 152 mm × 10.5 mm) to include sufficient thickness for the grooved design later on. First and foremost, multiple thicknesses for the normal rail pad (Figure 3.1) were proposed to study their effect on the rail pad's dynamic stiffness and energy dissipation. After that, the geometry of studs (Figure 3.2) and grooves (Figure 3.3) were studied to investigate their impact on the rail pad properties. The stud geometry was varied by changing the number of stud rows, stud diameter, and stud height. Each row of studs consisted of four studs that were spaced equally. Despite the studs' protrusion, the overall thickness of studded rail pad was still maintained at 10.5 mm. On the other hand, the groove geometry was varied by altering the number of grooves, groove depth, and groove width.

Moving on, the hole geometry (Figure 3.4) was then examined next to study the feasibility of material-saving design in rail pad. The holed design was defined by the number of hole rows and hole diameter. Similar to the studded design, each row has four holes that were equally spaced. Not only that, rail pad with square cut-out (Figure 3.5) at the centre that corresponds to 25.0%, 37.5%, 50.0%, and 62.5% of the side length (152 mm) was also proposed as an alternative to the holed design. Last but not least, the overall shape of the rail pad was also altered to the shape of circle (Figure 3.6) and various regular polygons (polygons with all sides equal) (Figure 3.7; Figure 3.8; Figure 3.9) to observe their effects on the rail pad properties. In this case, the thickness for all shapes was also the same at 10.5 mm. The size of the various rail pad shapes was not determined arbitrarily but they all shared the same area on the top surface. In short, there were six (6) rail pad designs investigated in this study, which is the normal, grooved, studded, cut-out, holed, and shaped designs.

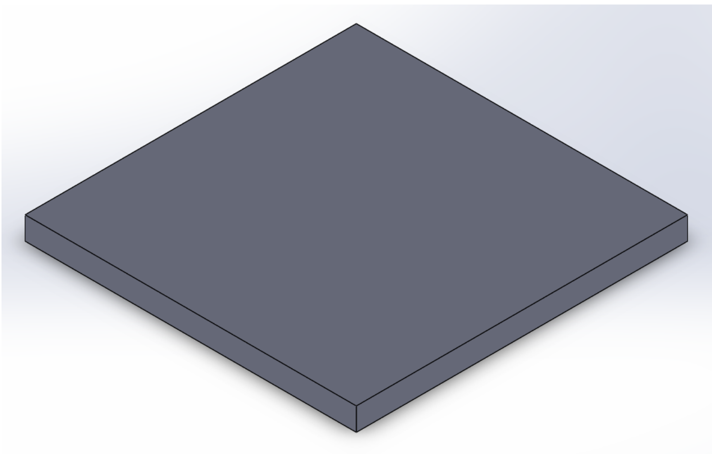

Figure 3.1: Normal Rail Pad

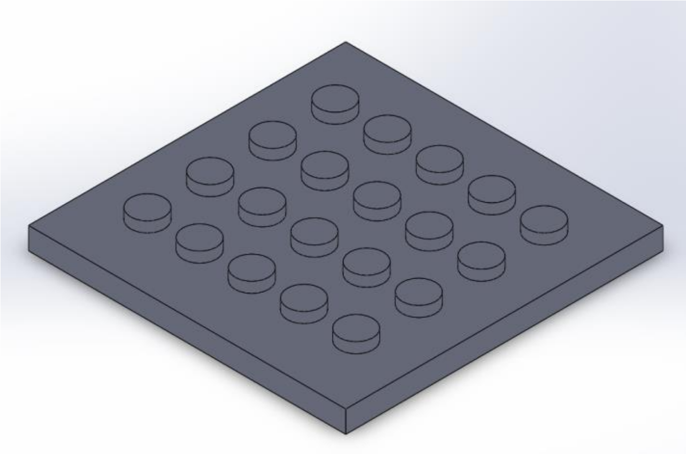

Figure 3.2: Studded Rail Pad

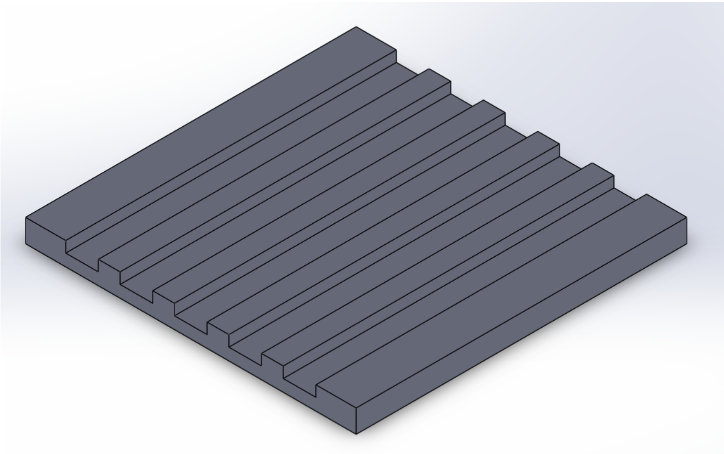

Figure 3.3: Grooved Rail Pad

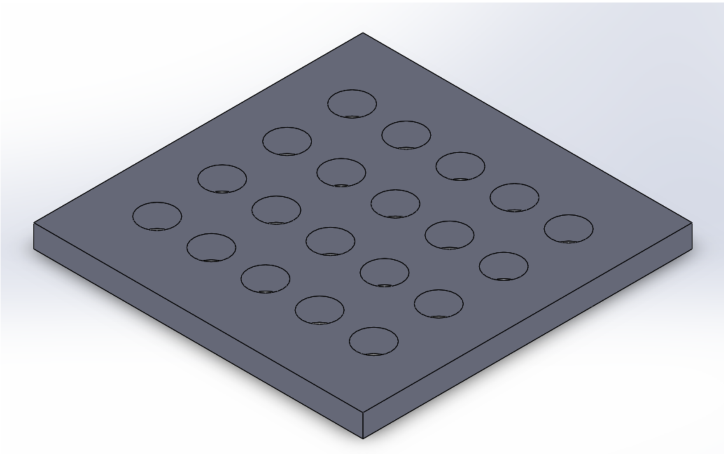

Figure 3.4: Holed Rail Pad

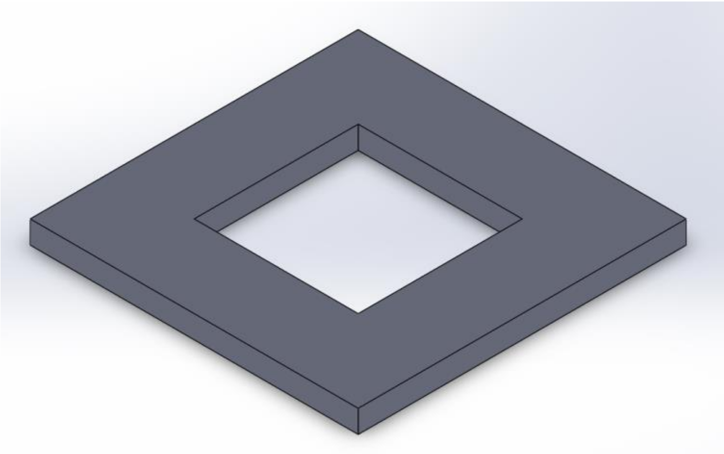

Figure 3.5: Cut-out Rail Pad

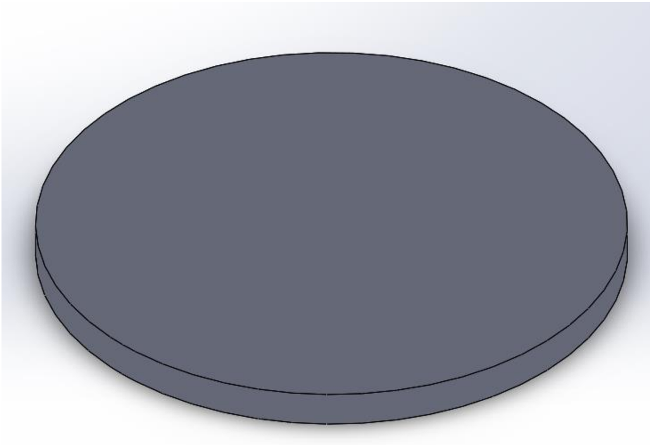

Figure 3.6: Circle Rail Pad

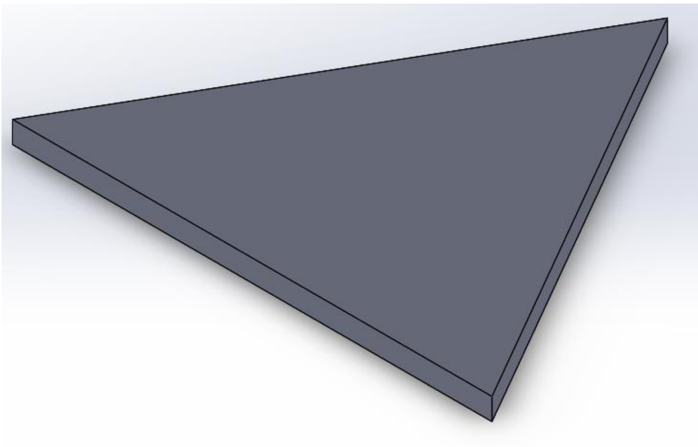

Figure 3.7: Triangle Rail Pad

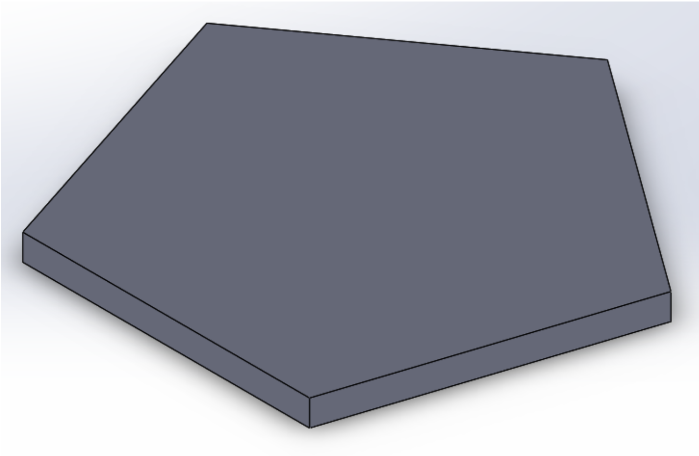

Figure 3.8: Pentagon Rail Pad

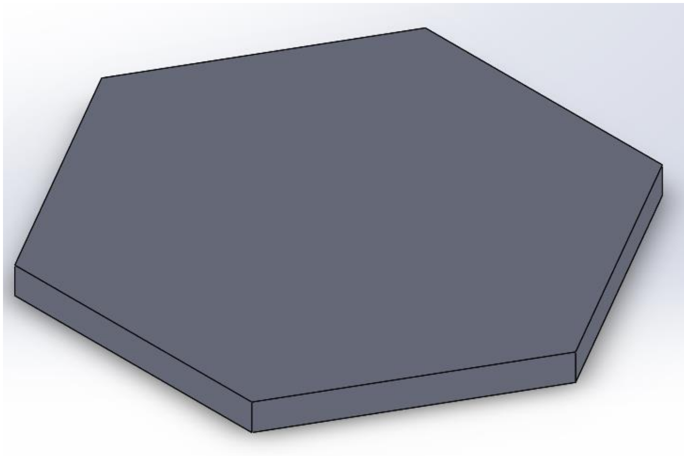

Figure 3.9: Hexagon Rail Pad

Only one feature of a given rail pad design was changed at a time to investigate its' influence on the dynamic stiffness and energy dissipation. Since there are many features that can be varied for the grooved, studded, and holed designs, a basic design was proposed for each of these three (3) rail pad designs; only the dimension of the feature that was under investigation was changed, and the other features followed the dimension of the basic design. The basic design itself was also a part of the proposed rail pad geometry and was simulated as well. As such, there were a total of 40 different rail pad geometries that were simulated. All the designs features, and dimensions considered in this study were tabulated and summarised in Table 3.2.

Table 3.2: Rail Pad Designs, Features, and Dimensions of the Study

Geometrical Features		Dimension
Design	Feature	
Normal	Thickness	4.5, 6.5, 8.5, 10.5, 12.5 mm
Studded	Basic Design	3 Rows of Studs of 20 mm Diameter and 2.0 mm Height
	Number of Rows	4, 5, 6
	Stud Diameter	24, 28, 32 mm
	Stud Height	3.5, 5.0, 6.5 mm
Grooved	Basic Design	3 Grooves with 2.0 mm Depth and 9 mm Width
	Number of Grooves	4, 5,6
	Groove Depth	3.5, 5.0, 6.5 mm
	Groove Width	12, 15, 18 mm
Holed	Basic Design	3 Rows of Holes of 10 mm Diameter
	Number of Rows	4, 5, 6
	Hole Diameter	13, 16, 19 mm
Cut-out	Cut-out Size	38 × 38 mm, 57 × 57 mm, 76 × 76 mm, 95 × 95 mm
Shaped	Circle	Radius = 85.76 mm
	Triangle	Side Length = 231.00 mm
	Pentagon	Side Length = 115.88 mm
	Hexagon	Side Length = 94.30 mm

3.5 Simulation Setup

At first, the CAD model of the different rail pad designs was drawn with SOLIDWORKS software. Since all rail pad designs are symmetrical, the quarter models and half models, models that are only one-fourth (1/4) and one-half (1/2) of the actual size, were used instead of the complete model to reduce computation time. The magnitude of the force loaded on the model was also divided to reflect the load on the quarter or half model. After that, the part files were converted into Parasolid files before transferring to the simulation software as part files are usually not directly accepted by them. In this study, ANSYS Transient Structural was used to simulate the time-dependent response of rail pad under the loading conditions stated previously. The material of cork rubber was prepared in the software by inserting the Prony series material data into the engineering data (Figure 3.10). In the geometry section, the Parasolid file of the rail pad was imported. Afterwards, in the model section, appropriately sized mesh was generated for the geometry. Fixed boundary condition was set at the bottom surface of the rail pad, while the loading was applied on the top surface where it forms contact with the rail. The load was set as a time-varying function according to Equation 3.1. Also, the top surface where the load is applied was set to rigid and constrained to only move in the vertical direction (direction of the loading) by applying the remote displacement setting. This was done to replicate the rough contact formed with the rail at the top surface of the rail pad that does not permit the surface to deform. Symmetry boundary conditions were also applied in the x- and y-directions as quarter or half models were used. The simulation simulated the loading for 2 s, which allowed the load to oscillate for ten (10) cycles for the periodic response to reach a steady state. A chart under the solution tab was created to plot out the force vs deformation graph of the rail pad, which takes the form of a hysteresis loop. The result data in the chart was then exported into text file for further computation and processing of the result. Figure 3.11 illustrates the simulation setup in the ANSYS Transient Structural.

Properties of Outline Row 3: Cork Rubber

	A	B	C	D	E
1	Property	Value	Unit		
2	Material Field Variables	Table			
3	Density	1150	kg m^-3		
4	Isotropic Elasticity				
5	Derive from	Bulk Modulus a...			
6	Young's Modulus	220.2	MPa		
7	Poisson's Ratio	0.4			
8	Bulk Modulus	367	MPa		
9	Shear Modulus	7.8643E+07	Pa		
10	Prony Volumetric Relaxation	Tabular			
11	Number of Terms	4			
12	Relative Moduli(i): Scale	1			
13	Relative Moduli(i): Offset	0			
14	Relaxation Time(i): Scale	1			
15	Relaxation Time(i): Offset	0	s		

	B	C	D
1	Index i	Relative Moduli(i)	Relaxation Time(i) (s)
2	1	0.1717	0.1
3	2	0.1362	0.01
4	3	0.218	0.001
5	4	0.1117	0.0001

Figure 3.10: Cork Rubber Material Data in ANSYS

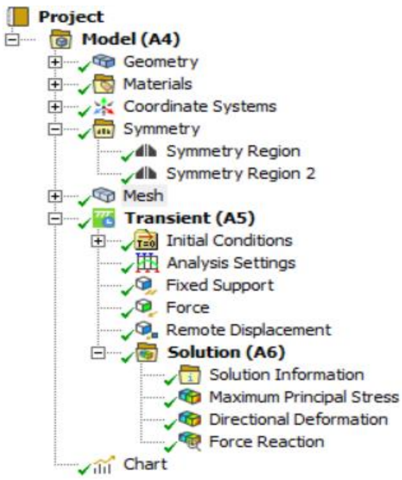

Figure 3.11: Simulation Setup in ANSYS Transient Structural

3.6 Result Data

Calculations are needed to compute the necessary values for the analysis of the result. Since the study's focus is on the dynamic stiffness and energy dissipation of rail pads, these two properties need to be derived from the simulation result so that the different geometrical features can be compared. In order to obtain the dynamic stiffness and energy dissipation, the simulation data were transferred to Microsoft Excel to plot out the force vs deformation graph (Figure 3.12) obtained from the simulation. In Excel, regression analysis was done to obtain the linear regression line of the graph. The gradient of the line was then taken as the dynamic stiffness of the rail pad. Subsequently, trapezoidal rule was used to calculate the area under the curve of the force vs deformation graph to obtain the energy dissipated by the rail pad. From there, the energy dissipated vs time graph (Figure 3.13) was plotted to obtain an oscillating graph with downward trend, indicating energy loss through damping. Regression analysis was done again on this graph to obtain the linear regression line. The gradient of the line was then taken and divided by ten (10) cycles to obtain the energy dissipation (average energy dissipated per cycle) of the rail pad.

As mentioned before, the geometrical features are introduced based on the baseline design (152 mm × 152 mm × 10.5 mm). Therefore, the dynamic stiffness and energy dissipation found for the different geometrical features are compared with those of the baseline design by computing the improvement ratio

(IR). Since there are two properties of the rail pad being studied, there are two (2) IRs for each dimension. The IR is calculated by the following formula:

$$IR = \frac{P_{feature}}{P_{baseline}} \tag{3.3}$$

Where IR is the improvement ratio. $P_{feature}$ is the property (dynamic stiffness or energy dissipation) for the rail pad with a certain geometrical feature, while $P_{baseline}$ is the property (dynamic stiffness or energy dissipation) of the baseline design. By using the IR, one can easily deduce if a certain feature improves or degrades the dynamic stiffness or energy dissipation of the rail pad.

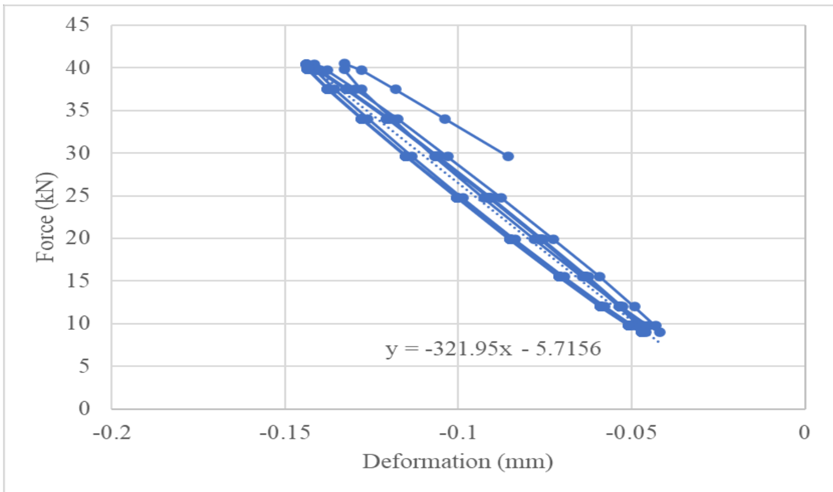

Figure 3.12: Force vs Deformation Graph

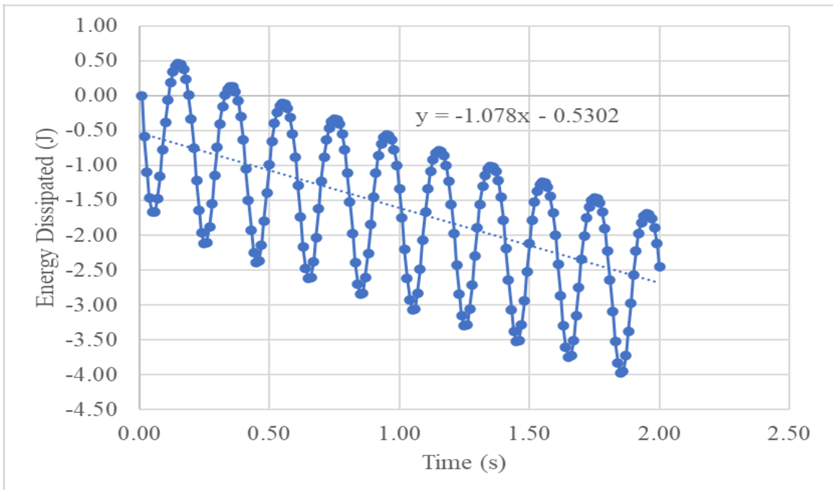

Figure 3.13: Energy Dissipated vs Time Graph

3.7 Work Plan

The project flow for this study is outlined in Figure 3.14. This project first started with the review of existing researches to gather information on the literature review section. After that, with sufficient background knowledge, the material data for the rubber material and the loading conditions used were referred from the reviewed sources. Subsequently, the simulation software used in this study and setup necessary were planned and outlined. Afterwards, the rail pad designs and features that are interested were determined, and multiple dimensions were proposed for each of the features in each rail pad design. At this point, the methodology was completely planned. The CAD models for each of the rail pad geometries were then drawn for the simulation.

With the CAD model prepared, simulation was carried out for a particular rail pad design with a certain feature and dimension to obtain the force vs deformation data. From the data, the dynamic stiffness, energy dissipation, and IR were computed. After that, if there were still any remaining rail pad geometry untested, the steps returned back to performing simulation for that geometry. Once all the rail pad geometries have been simulated, the project proceeded to the result and discussion section.

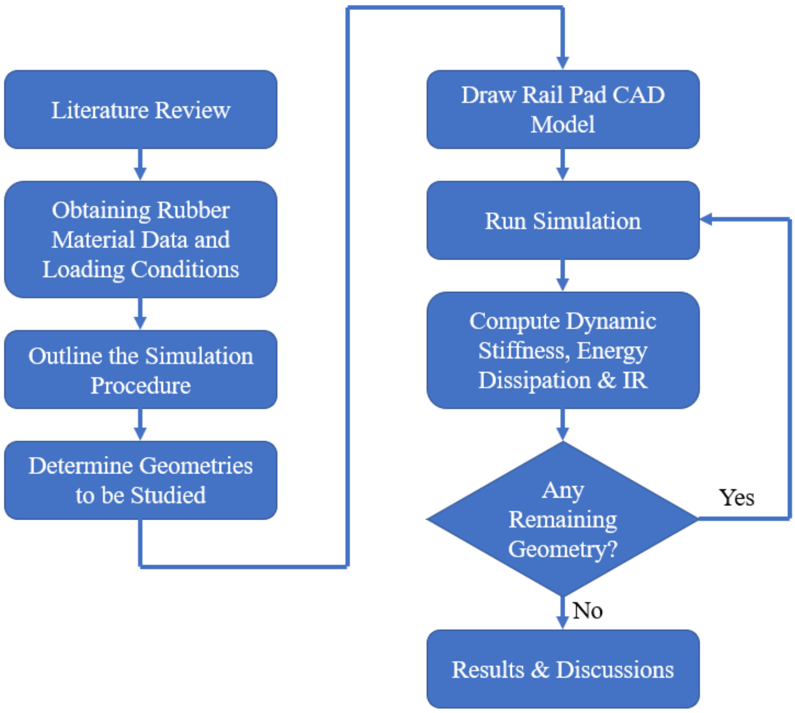

Figure 3.14: Project Flow of the Project

3.8 Summary

This chapter outlines the details and procedure of the simulation that were conducted to obtain the result of this study. The rubber material data used was for cork rubber which is the material for making FC9 rail pads. The loading condition was referenced from other source to consist of 31.5 kN, 5 Hz dynamic, and 18 kN static loads. Various geometrical features and rail pad designs with different dimensions were proposed to be studied with simulation. The rail pad designs included the normal, studded, grooved, holed, square cut-out, and shaped rail pad designs. ANSYS Transient Structural software was used to run the simulation and plot the force vs deformation graph. From the graph, the dynamic stiffness, energy dissipation, and improvement ratio (IR) were then calculated for the upcoming chapter.

CHAPTER 4

RESULTS AND DISCUSSIONS

4.1 Introduction

After the simulations were done, the dynamic stiffness and energy dissipation of the different rail pad geometries were computed and graphed to observe the overall trend of the properties with changing rail pad dimensions. Since the quarter and half models were used in the simulations, the dynamic stiffness and energy dissipation obtained from the graphs were multiplied by 4 (for quarter model) and 2 (for half model) respectively to obtain the actual value of the properties for the complete model. Also, it should be made clear that "dynamic properties" in this chapter and Chapter 5 (Conclusions and Discussions) refers to the dynamic stiffness and energy dissipation collectively.

4.2 Normal Rail Pad

Figure 4.1 illustrates the dynamic stiffness and energy dissipation of normal rail pads according to their thickness. From the figure, the dynamic stiffness exhibited a decreasing trend when the thickness increased. As the thickness increased from 4.5 mm to 10.5 mm, the dynamic stiffness dropped significantly from 1534.96 kN/mm to 646.60 kN/mm. This observation correlates with the findings of Sol-Sanchez, Moreno-Navarro and Rubio-Gamez (2014), and Zakeri et al. (2021) who confirmed that increasing the thickness of rail pad/rubber sheet decreases their dynamic stiffness. On the other hand, the energy dissipation exhibited an increasing trend as the thickness increased, which also agrees with the observations from Sol-Sanchez, Moreno-Navarro and Rubio-Gamez (2014). The energy dissipation increased from 0.0975 J to 0.2553 J as the thickness increased from 4.5 mm to 10.5 mm.

As inspired by the findings from Sol-Sanchez, Moreno-Navarro and Rubio-Gamez (2014), curve fitting was carried out to explore the possible relation between dynamic stiffness and energy dissipation with thickness. Different trendline options were available in Microsoft Excel, which are exponential, linear, logarithmic, polynomial, and power law models. The trendline for each dynamic property is selected based on the highest determination of coefficient, R^2. However, if the datapoints clearly suggest a straight line on the graph, a linear trendline is chosen regardless of the R^2 value as the linear equation is simpler.

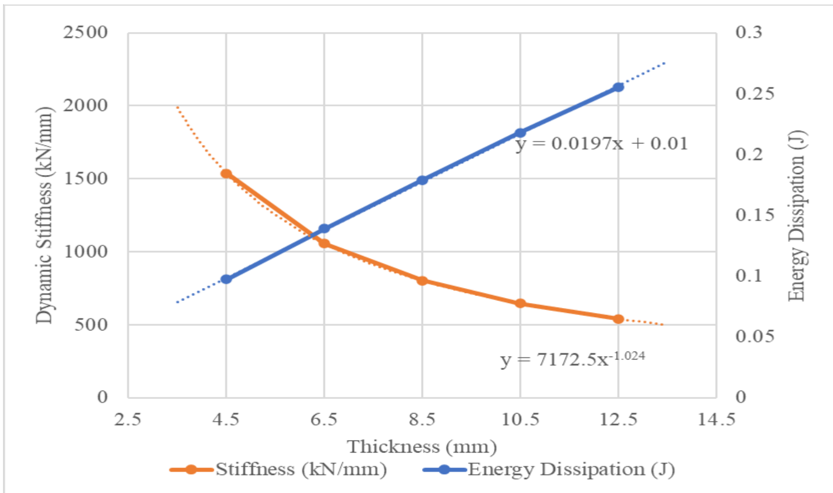

Figure 4.1: Properties of normal rail pad with varying thickness

For dynamic stiffness, the power law model has the highest R^2 value, thus suggesting that the relation between dynamic stiffness and thickness is best represented by the power law. This observation also correlates with the findings of Sol-Sanchez, Moreno-Navarro and Rubio-Gamez (2014) who reported that both static and dynamic stiffnesses can be well fitted with power law. Since the index of the power law model found in this study is -1.024, this means that the model closely resembles the reciprocal function, and the dynamic stiffness is essentially just inversely proportional to the thickness. This, however, contradicts with the results from Sol-Sanchez, Moreno-Navarro and Rubio-Gamez (2014) as the index they calculated is -2.349 instead. A possible explanation for this discrepancy could be the rail pad material is different in the literature compared to the material in this study. As for the energy dissipation, it is very clear that the energy dissipation plot in Figure 4.1 takes the form of a straight line. Therefore, it was concluded that the energy dissipation of normal rail pad is essentially linearly proportional to the thickness.

As mentioned previously, all the results of the proposed rail pad dimensions were compared to that of the baseline design by computing the improvement ratio (IR). Table 4.1 shows the IRs for the different thickness of normal rail pad. Since the baseline design is the normal rail pad with 10.5 mm thickness, its' IR of dynamic stiffness and energy dissipation are equal to exactly 1.000. From the table, it can be observed that dynamic stiffness varied significantly with changes in thickness such that it reached up to more than twice the amount (4.5 mm) of the baseline design as thickness decreased. Similarly, the energy dissipation also varied significantly where it reduced to less than half (4.5 mm) of the baseline design when thickness decreased. The substantial changes in dynamic stiffness and energy dissipation as a result of thickness variation suggests that thickness is a significant feature in deciding the dynamic properties for rail pads of any geometry.

Table 4.1: Improvement Ratios of the Normal Rail Pad

Normal	4.5 mm	6.5 mm	8.5 mm	10.5 mm	12.5 mm
Stiffness (kN/mm)	2.376	1.635	1.243	1.000	0.835

Normal	4.5 mm	6.5 mm	8.5 mm	10.5 mm	12.5 mm
Energy Dissipation (J)	0.448	0.637	0.821	1.000	1.172

4.3 Studded Rail Pad

Studded rail pad design was investigated in this study to understand the impact of stud geometry on the rail pad's dynamic stiffness and energy dissipation. This rail pad design was studied because it is widely used in the real world yet receiving little to no attention in the literature on its' effect on the rail pad's dynamic properties. Therefore, in this study, the dimensions of the stud geometry on studded rail pad were varied to observe the variation in dynamic properties as dimension changes. The features that were under investigation for the studded rail pad are the stud diameter, stud height, and number of stud rows.

Figure 4.2 shows the graph of the dynamic stiffness and energy dissipation as the stud diameter varies. It should be noted that, for all the rail pad designs that has multiple features, the result of the basic design is also compared with that of the various proposed dimensions of each feature, and the basic design's dimension is always smaller than all the proposed dimensions for all features. Hence, there are four (4) data points in Figure 4.2 despite only three

(3) stud diameters proposed in Table 3.2; the 20 mm stud diameter in Figure 4.2 is the dimension of the basic design.

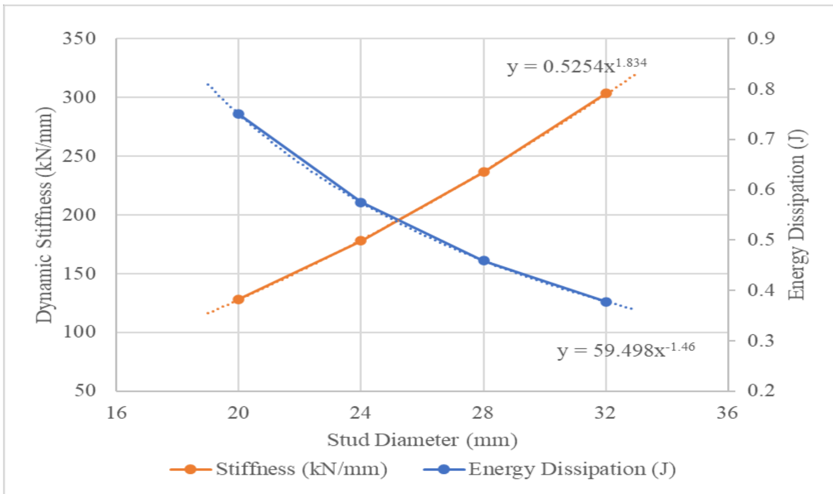

Figure 4.2: Properties of studded rail pad with varying stud diameter

By comparing dynamic stiffness of basic design (20 mm stud diameter) with the baseline design, it was clear that the introduction of studs has a massive softening effect on the studded rail pad. The dynamic stiffness of the basic design was only 128.18 kN/mm as compared to 646.40 kN/mm for the baseline design. When looking at the energy dissipation, it seemed that the presence of studs considerably elevated the energy dissipation of studded rail pad. The energy dissipation of basic design was 0.7499 J as compared to only 0.2178 J for baseline design. Based on Figure 4.2, the dynamic stiffness was shown to increase as the stud diameter became larger. The dynamic stiffness increased from 128.18 kN/mm to 303.49 kN/mm as stud diameter increased from 20 mm to 32 mm. In contrast to dynamic stiffness, the energy dissipation appeared to decrease when stud diameter increased. The energy dissipation reduced from 0.7499 J to 0.3776 J as the stud diameter increased from 20 mm to 32 mm. When trendlines were created for the graphs, it was realised that both the dynamic stiffness and energy dissipation are best represented by the power law when the stud diameter is changed.

Figure 4.3 shows the graph of dynamic stiffness and energy dissipation as the stud height varies. From the figure, the dynamic stiffness was shown to decrease as the stud height increased. The dynamic stiffness reduced from

128.18 kN/mm to 106.33 kN/mm as stud height increased from 2.0 mm to 6.5 mm. Meanwhile, the energy dissipation increased initially with increasing stud height before it peaked and then decreased with further increment in stud height. The energy dissipation increased from 0.7499 J at 2.0 mm, peaked at 0.8027 J at 5.0 mm, and then decreased to 0.7798 J as the stud height reached 6.5 mm. For dynamic stiffness, the linear equation is the most suitable in representing its's relation with stud height. As for energy dissipation, its' relation with stud height can be represented by the quadratic equation due to the presence of peak.

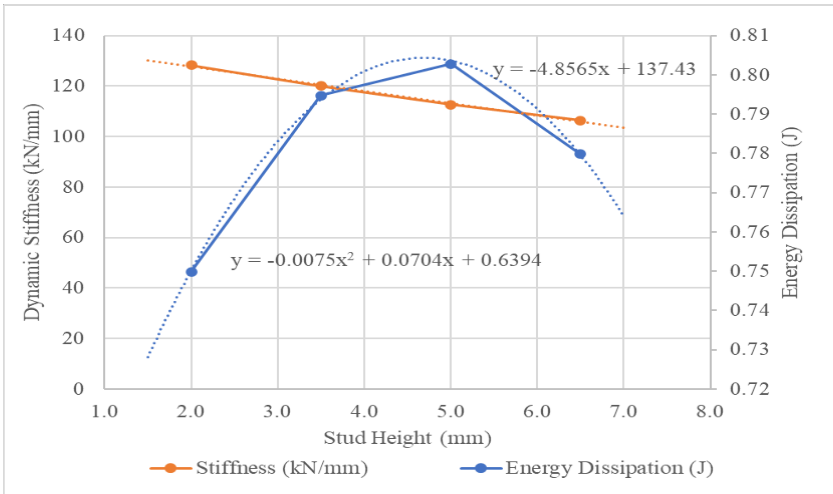

Figure 4.3: Properties of studded rail pad with varying stud height

Figure 4.4 shows the graph of dynamic stiffness and energy dissipation as more stud rows are added. Based on the figure, the dynamic stiffness exhibited an increasing trend as the number of stud rows increased. The dynamic stiffness increased from 128.18 kN/mm at 3 stud rows to 251.88 kN/mm at 6 stud rows. On the other hand, the energy dissipation showed a decreasing trend as stud rows increased. The energy dissipation reduced from 0.7499 J at 3 rows to 0.4027 J at 6 rows. The linear equation is the best in describing the relation of dynamic stiffness when the number of stud rows is varied. In other words, dynamic stiffness is linearly proportional to the number of stud rows. As for energy dissipation, the quadratic equation best describes its' relation with the number of stud rows.

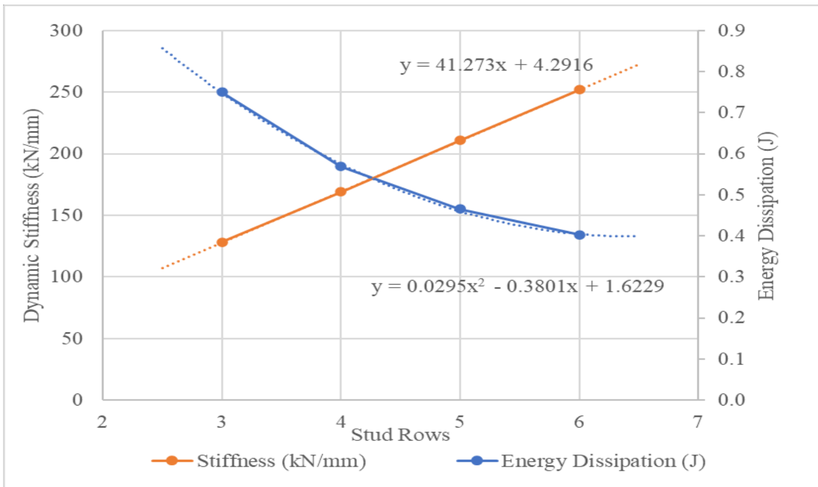

Figure 4.4: Properties of studded rail pad with varying stud rows

Table 4.2 shows the IRs of the different features and dimensions of the studded rail pad. From the table, it can be seen that the features that significantly influence both dynamic stiffness and energy dissipation are the stud diameter and number of stud rows where the stud diameter is the most influential among all features. Meanwhile, stud height only affected little on dynamic properties. This data suggested that the stud diameter and number of stud rows require the most attention while designing studded rail pad as the dynamic properties are most sensitive to these parameters. Moreover, despite the increase in dynamic stiffness and decrease in energy dissipation due to stud diameter enlargement or stud row addition, the dynamic properties were still far from being close to that of the baseline design. This indicated a limit to which the dynamic properties of studded rail pad can be attenuated by the stud diameter and number of stud rows.

Table 4.2: Improvement Ratios of the Studded Rail Pad

Studded	20 mm	24 mm	28 mm	32 mm	Stud Diameter
Stiffness (kN/mm)	0.198	0.275	0.366	0.470	
	2.0 mm	3.5 mm	5.0 mm	6.5 mm	Stud Height
	0.198	0.186	0.174	0.164	
	3	4	5	6	Stud Rows
	0.198	0.262	0.326	0.390	

Studded	20 mm	24 mm	28 mm	32 mm	Stud Diameter
Energy Dissipation (J)	3.443	2.640	2.107	1.734	
	2.0 mm	3.5 mm	5.0 mm	6.5 mm	Stud Height
	3.443	3.649	3.686	3.581	
	3	4	5	6	Stud Rows
	3.443	2.613	2.137	1.849	

4.4 Grooved Rail Pad

Grooved rail pad design was also investigated to find out the impact of groove geometry on the rail pad's dynamic stiffness and energy dissipation. Similar to the studded rail pad, the grooved rail pad is widely used in the railway industry; however, there are no existing researches studying the effect of grooves on the rail pad's dynamic properties. Thus, the influences of grooves on the dynamic properties were also investigated in this study. For grooved rail pad, the features that were studied were the groove depth, number of grooves, and groove width.

Figure 4.5 depicts the trend of dynamic stiffness and energy dissipation as the depth of groove varies. Similar to studs, the addition of grooves on the basic design (2.0 mm groove depth) resulted in softening of its' dynamic stiffness although not as much as the impact of studs. The dynamic stiffness of the basic design has only reduced from 646.40 kN/mm (baseline) to 550.48 kN/mm (basic) as a result of grooves addition. Besides, the energy dissipation of the basic design also increased slightly due to the groove feature. Energy dissipation of basic design increased from 0.2179 J (baseline) to 0.2306 J (basic). Referring to Figure 4.5, the dynamic stiffness reduced as the groove depth increased. Dynamic stiffness reduced from 550.48 kN/mm to 518.68 kN/mm as the groove depth deepened from 2.0 mm to 6.5 mm. Furthermore, the energy dissipation grew initially and finally declined after reaching a peak as groove depth increased. Energy dissipation grew from 0.2306 J (2.0 mm) to 0.2319 J (3.5 mm) before declined to 0.2284 J (6.5 mm). As for the trendline of the dynamic properties, relation between dynamic stiffness and groove depth is simply described by linear equation, and the dynamic stiffness is directly proportional to groove depth. Due to the presence of peak, the energy dissipation is thus related with the groove depth by the quadratic equation.

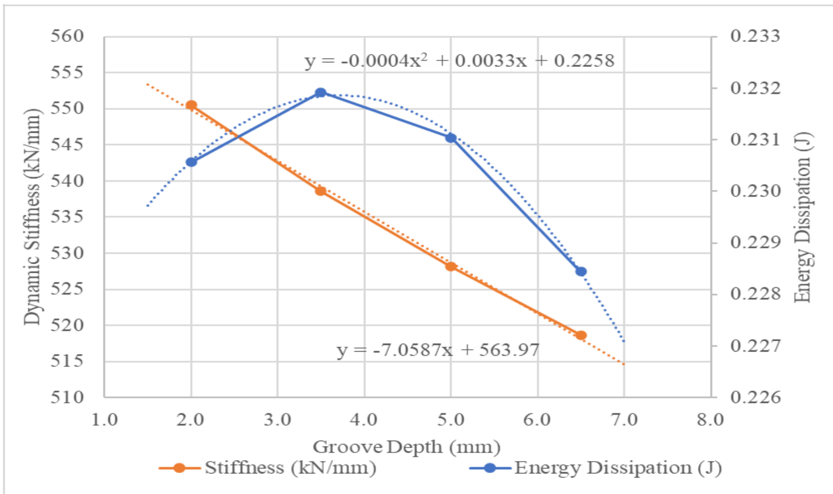

Figure 4.5: Properties of grooved rail pad with varying groove depth

Figure 4.6 depicts the trend of dynamic stiffness and energy dissipation as the number of grooves changes. Based on Figure 4.6, the dynamic stiffness declined as more grooves were added to the rail pad. The dynamic stiffness declined from 550.48 kN/mm with 3 grooves to 457.52 kN/mm with 6 grooves. On the other hand, the energy dissipation rose as more grooves were added to the rail pad. Energy dissipation rose from 0.2306 J with 3 grooves to 0.2445 J with 6 grooves. When the number of grooves was altered, it was observed that both dynamic stiffness and energy dissipation can be related with the groove number by the linear equation, and both properties are directly proportional to groove number.

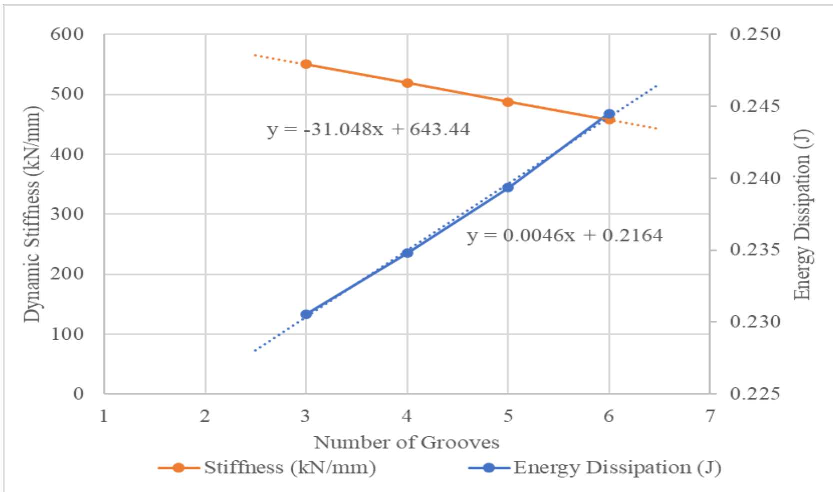

Figure 4.6: Properties of grooved rail pad with varying number of grooves

Figure 4.7 depicts the trend of dynamic stiffness and energy dissipation as groove width becomes bigger. According to the figure, the dynamic stiffness displayed a declining trend as the groove width enlarged. The dynamic stiffness reduced from 550.48 kN/mm to 430.48 kN/mm as groove width increased from 9 mm to 18 mm. In addition, the energy dissipation showed a rising trend as groove width increased. The energy dissipation rose from 0.2306 J to 0.2685 J as groove width increased from 9 mm to 18 mm. From the Figure, it was seen that the dynamic stiffness correlates well with the linear equation, indicating that it is directly proportional to the number of grooves. Meanwhile, the energy dissipation is not quite linear and better represented by a quadratic equation when the groove width is changed.

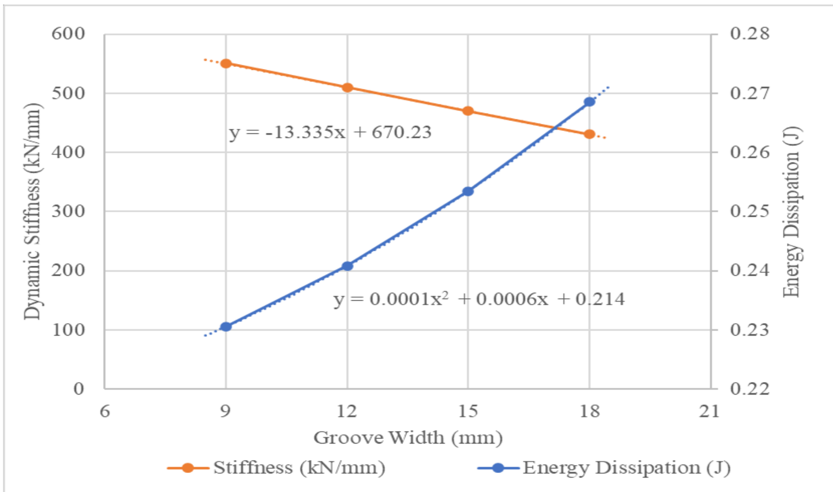

Figure 4.7: Properties of grooved rail pad with varying groove width

Table 4.3 shows the IRs of the proposed features and dimensions of the grooved rail pad studied. Based on the IRs, groove width has the most impactful effect on both dynamic properties of grooved rail pad. Not only that, the number of grooves also produced considerable effect on dynamic stiffness but only minorly affected the energy dissipation. In contrast, the groove depth has the smallest impact on dynamic stiffness among the discussed features and has almost no influence on energy dissipation. Therefore, the groove width and number of grooves are the significant factors that should be considered during the design of grooved rail pad. In addition, the increase of groove depth, grooves number, and groove width only softens dynamic stiffness. Meanwhile, the increase of groove number and groove width only enhances energy dissipation, while groove depth has minimal effect on energy dissipation. These showed that the loss of dynamic stiffness and gain of energy dissipation due to grooves creation on the normal rail pad (baseline design) cannot be compensated by adjusting the groove geometry other than totally eliminating the groove features.

Table 4.3: Improvement Ratios of the Grooved Rail Pad

Grooved	2.0 mm	3.5 mm	5.0 mm	6.5 mm	Groove Depth
Stiffness (kN/mm)	0.852	0.833	0.817	0.802	
	3	4	5	6	Groove Number
	0.852	0.803	0.754	0.708	
	9 mm	12 mm	15 mm	18 mm	Groove Width
	0.852	0.789	0.727	0.666	

Grooved	2.0 mm	3.5 mm	5.0 mm	6.5 mm	Grooved Depth
Energy Dissipation (J)	1.059	1.065	1.061	1.049	
	3	4	5	6	Groove Number
	1.059	1.078	1.099	1.123	
	9 mm	12 mm	15 mm	18 mm	Groove Width
	1.059	1.106	1.164	1.233	

4.5 Holed Rail Pad

Holed rail pad was studied to determine the impact of hole geometry on the rail pad’s dynamic stiffness and energy dissipation. The holed design was proposed to reduce the amount of material on the rail pad in order to save up on material cost and increase the cost-effectiveness of rail pad. Since the hole geometry on the rail pad is likely to alter the dynamic properties, the influences due to the presence of holes was studied to better understand the dynamic properties trend as hole geometry changed. For the holed rail pad, the features considered in this study were the hole diameter and number of hole rows.

Figure 4.8 is the graph of the dynamic stiffness and energy dissipation of the rail pad as the hole diameter changes. The introduction of holes on the basic design (10 mm hole diameter) caused a small decrement in dynamic stiffness. The dynamic stiffness of the basic design was 609.36 kN/mm as compared to 646.40 kN/mm of the baseline design. Also, the energy dissipation decreased only very slightly as holes were introduced on the rail pad. The energy dissipation of the basic design was 0.2147 J as compared to 0.2178 J for the baseline design. From Figure 4.8, the dynamic stiffness reduced as hole diameter enlarged. The dynamic stiffness reduced from 609.36 kN/mm to

528.04 kN/mm as hole diameter increased from 10 mm to 19 mm. Moreover, the energy dissipation also rose as hole diameter became larger. The energy dissipation rose from 0.2147 J to 0.2214 J as hole diameter increased from 10 mm to 19 mm. Furthermore, both dynamic stiffness and energy dissipation follow the quadratic equation when the hole diameter is altered.

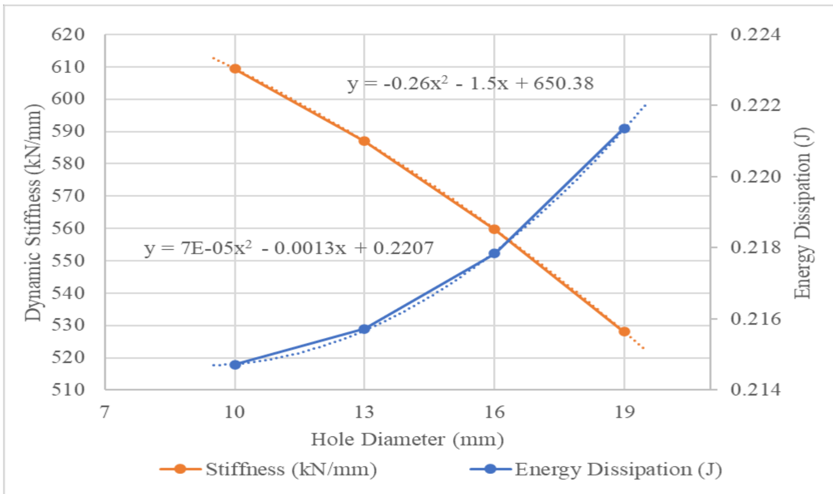

Figure 4.8: Properties of holed rail pad with varying hole diameter

Figure 4.9 shows the trend of the dynamic stiffness and energy dissipation as more hole rows are added. Based on the figure, the dynamic stiffness displayed a decreasing trend as the number of hole rows increased. The dynamic stiffness dropped from 609.36 kN/mm to 574.12 kN/mm as the number of hole rows increased from 3 rows to 6 rows. In addition, the energy dissipation also displayed a decreasing trend as more rows of holes were added. The energy dissipation declined from 0.2147 J at 3 rows to 0.2125 J at 6 rows. Based on the trendline, the dynamic stiffness relates to the number of hole rows by linear equation, indicating a directly proportional relation. For the energy dissipation, it follows a quadratic equation as the number of hole rows changes.

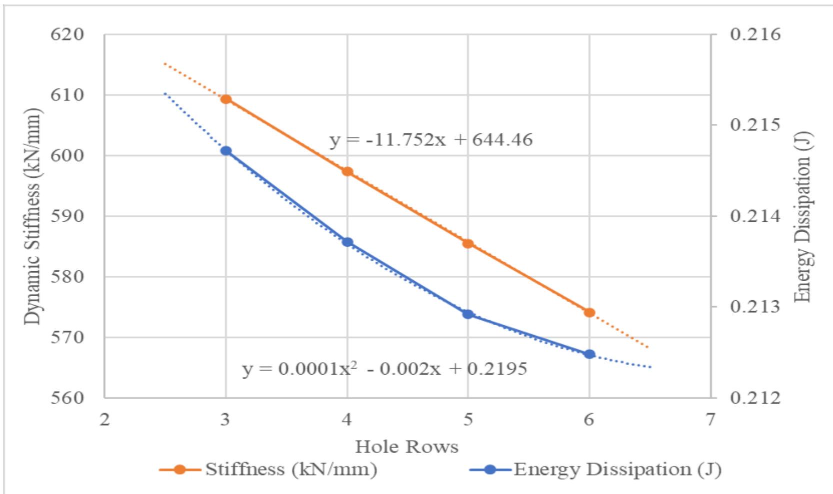

Figure 4.9: Properties of holed rail pad with varying number of hole rows

Table 4.4 tabulates the IRs calculated for the different features and dimensions of holed rail pad. From the result shown, hole diameter has greater effect on dynamic stiffness of holed rail pad than the number of hole rows. Still, both features have considerable impact on the dynamic stiffness. Meanwhile, the energy dissipation was essentially unaffected by both the hole diameter and number of hole rows. Hence, the introduction of holes on the rail pad mainly influences only its' dynamic stiffness, and the hole diameter is the most significant feature in influencing this property. Moreover, the dynamic stiffness also only declined as hole diameter enlarged or number of hole rows increased, demonstrating that the holed rail pad always has lower dynamic stiffness than the no-hole rail pad (baseline design).

Table 4.4: Improvement Ratios of the Holed Rail Pad

Holed	10 mm	13 mm	16 mm	19 mm	Hole Diameter
Stiffness (kN/mm)	0.943	0.908	0.866	0.817	
	3	4	5	6	Hole Rows
	0.943	0.924	0.906	0.888	

Holed	10 mm	13 mm	16 mm	19 mm	Hole Diameter
Energy Dissipation (J)	0.986	0.990	1.000	1.016	
	3	4	5	6	Hole Rows
	0.986	0.981	0.978	0.976	

4.6 Cut-out Rail Pad

Cut-out rail pad was also studied to understand the effect of square cut-out on the dynamic stiffness and energy dissipation of the rail pad. This design was proposed to serve as an alternative to the holed design for reducing material cost and improving cost-effectiveness of the rail pad. The cut-out design only has one feature to be altered, which is the length / width of the square cut-out.

Figure 4.10 illustrates the dynamic stiffness and energy dissipation as the size of the square cut-out increases. Similar to the holed rail pad, the cutting out of the rail pad centre produced a small reduction in the dynamic stiffness of the basic design (38 mm cut-out size). The dynamic stiffness of the basic design reduced to 599.20 kN/mm from 646.40 kN/mm of the baseline design as cut-out was created. In contrast to the observation of holed rail pad, energy dissipation of cut-out basic design rose slightly rather than dropping. The energy dissipation of the basic design was 0.2247 J as compared to 0.2178 J of the baseline design. According to the figure, the dynamic stiffness decreased significantly as the cut-out size grew. The dynamic stiffness decreased from 599.20 kN/mm to 374.78 kN/mm as cut-out size grew from 38 mm to 95 mm. On the other hand, the energy dissipation also increased substantially as cut-out became larger. The energy dissipation increased from 0.2247 J to 0.2981 J as cut-out size increased from 38 mm to 95 mm. As for the trendline, both the dynamic stiffness and energy dissipation are well represented by the quadratic equation.

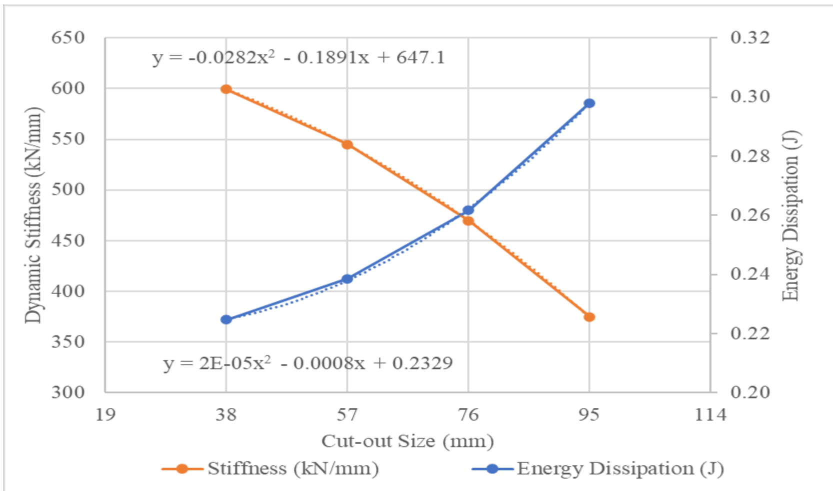

Figure 4.10: Properties of cut-out rail pad with varying cut-out size

Table 4.5 tabulates the IRs for the proposed dimensions of cut-out rail pad investigated in this study. From the table, it was also seen that the dynamic stiffness was significantly reduced with the cut-out feature to the point that the dynamic stiffness is only 58.0% of the baseline design. Similarly, the energy dissipation was also substantially improved up to 136.9% of the baseline design. This result demonstrated that the cut-out feature is also a significant feature in altering rail pad's dynamic properties when compared to stud, groove, and hole features.

Table 4.5: Improvement Ratios of the Cut-out Rail Pad

Cut-out	38 mm	57 mm	76 mm	95 mm	Cut-out Size
Stiffness (kN/mm)	0.927	0.843	0.727	0.580	

Cut-out	38 mm	57 mm	76 mm	95 mm	Cut-out Size
Energy Dissipation (J)	1.032	1.095	1.201	1.369	

Since the cut-out and holed rail pads were introduced to save material, the material saving between both designs are compared. The comparison was done by calculating the dynamic property changes per unit volume, which is the ratio of the absolute difference between the properties of baseline design and those of each feature, and the material volume removed by the holes or cut-out. Table 4.6 tabulates the volumetric dynamic property changes for all features of holed and cut-out rail pads. If the volumetric dynamic property change is small, it indicates a higher material saving capacity as more material can be removed while only affecting little on the dynamic properties; lesser adjustment to other geometry is needed to compensate the dynamic properties loss or gain as a result of the hole and cut-out features. In Table 4.6, the volumetric dynamic stiffness changes for cut-out rail pad are smaller than those of holed rail pads, indicating that cut-out design is more suitable for material saving consideration. However, the opposite was observed when looking at the volumetric energy dissipation changes where holed rail pads have lower values. As discussed in the literature review, dynamic stiffness is crucial for rail pad; thus, focus should be on creating lesser impact on the dynamic stiffness while the material-removing features are produced. In other words, the cut-out design has higher material saving capacity than the holed design for the application of rail pad.

Table 4.6: Dynamic Property Changes per Unit Volume of Holed and Cut-out Rail Pads

Dynamic Stiffness Change per Unit Volume (kN/mm^4) (10^{-3})					
Holed Rail Pad	10 mm	13 mm	16 mm	19 mm	Hole Diameter
	3.74	3.55	3.42	3.31	
	3	4	5	6	Hole Rows
	3.74	3.72	3.69	3.65	
Cut-out Rail Pad	38 mm	57 mm	76 mm	95 mm	Cut-out Size
	3.11	2.98	2.91	2.87	

Energy Dissipation Change per Unit Volume (J/mm^3) (10^{-7})					
Holed Rail Pad	10 mm	13 mm	16 mm	19 mm	Hole Diameter
	3.11	1.24	0.0158	0.997	
	3	4	5	6	Hole Rows
	3.11	3.09	2.96	2.69	
Cut-out Rail Pad	38 mm	57 mm	76 mm	95 mm	Cut-out Size
	4.56	6.07	7.23	8.47	

4.7 Shaped Rail Pad

Shaped rail pad was also studied to investigate the effect of different rail pad shape on its' dynamic stiffness and energy dissipation. This category of rail pad design was experimented to determine if there are any benefits associated with changing rail pad shape, while maintaining the same top surface area and thickness. The shapes proposed were the triangle, square (baseline design), pentagon, hexagon, and circle.

Figure 4.11 depicts the dynamic stiffness and energy dissipation of rail pads of different shape. In the figure, the rail pad shapes were arranged in increasing vertices where triangle was placed first as it has only three (3) vertices. Circle was placed last as it can be taken as a polygon with infinite vertices. From the graph, both the dynamic stiffness and energy dissipation increased from 643.90 kN/mm and 0.2156 J to 647.14 kN/mm and 0.2185 J respectively as rail pad shape changed from triangle to pentagon. After that, the dynamic properties dropped to 646.96 kN/mm and 0.2183 J respectively as the shape was changed to hexagon before increasing to 648.08 kN/mm and 0.2192 J respectively for circle rail pad. Even though the rail pad shape did influence the dynamic properties, the properties only fluctuated in a very tight range, which was around 643 kN/mm to 649 kN/mm for dynamic stiffness and 0.2150 J to 0.2200 J for energy dissipation.

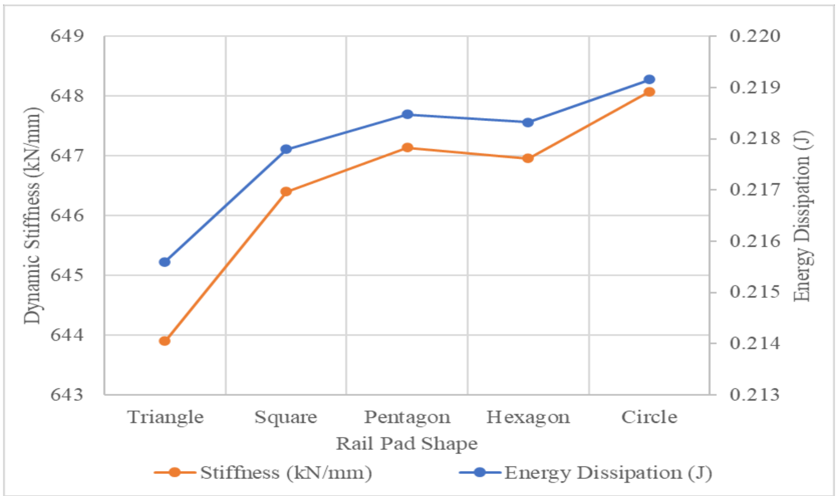

Figure 4.11: Properties of rail pad of different shape

Table 4.7 shows the IRs of the dynamic properties calculated for the different rail pad shape. By comparing the dynamic properties relative to the square rail pad (baseline design), it was evident that the changes resulted to the dynamic properties due to different rail pad shape is very insignificant. The largest difference between IRs of the shaped rail pad and those of the baseline design was only -0.4% (triangle) for dynamic stiffness and -1.0% (triangle) for energy dissipation. Therefore, it was concluded that the rail pad shape does not affect the dynamic properties by a significant margin, and the shape of rail pad should be chosen as whichever is the cheapest or convenient to manufacture during the rail pad design.

Table 4.7: Improvement Ratios of the Shaped Rail Pad

Shaped	Triangle	Square	Pentagon	Hexagon	Circle
Stiffness (kN/mm)	0.996	1.000	1.001	1.001	1.003

Shaped	Triangle	Square	Pentagon	Hexagon	Circle
Energy Dissipation (J)	0.990	1.000	1.003	1.002	1.006

4.8 Overview of all Rail Pad Designs

Figure 4.12 and Figure 4.13 show the range of the IR for both properties of all the rail pad features and designs discussed in this study. Referring to the IR range of dynamic stiffness, it was concluded that only the rail pad thickness can effectively amplify dynamic stiffness. The studded, grooved, holed, and cut-out designs only degraded the dynamic stiffness, while changing rail pad shape produced only very minute stiffening effect when pentagon, hexagon or circle shape is adopted. Although certain features, such as stud diameter and stud rows, can increase dynamic stiffness, it was still limited and cannot exceed that of the normal rail pad of the same overall thickness and area (baseline design) as discussed in previous sections. Hence, during the design stage, thickness should be adjusted to create a higher dynamic stiffness so as to compensate the softening effect due to these features. Meanwhile, the opposite trend was observed for energy dissipation. The thickness is the only feature that can significantly reduce energy dissipation of the rail pad. The studded, grooved, and cut-out designs only enhanced the energy dissipation, while holed and shaped designs barely affected it.

From the figures, it also showed that the thickness is the most significant feature of all, capable of creating large variation in the dynamic properties. The second most significant feature/design is the stud features or studded design where its' dynamic stiffness is also massively reduced, while energy dissipation is greatly elevated as studs are introduced to the rail pad. Moving on, the third most significant feature/design is the cut-out feature/design which also displayed substantial reduction in dynamic stiffness and elevation in energy dissipation.

In general, the introduction of all the features discussed in this study except hole and shape resulted in the trading-off of dynamic stiffness for more energy dissipation. For the application of rail pad, the gaining of energy dissipation is not critical as it is more important for the dynamic stiffness to suit the application of the railway. Therefore, priority should be given to the change in dynamic stiffness while designing rail pad geometry, and attenuation to the energy dissipation associated with the rail pad features is just a secondary consequence. Due to the significant influence of rail pad thickness, the thickness is a suitable and simple feature to be altered for adjusting the rail pad properties. However, the cut-out feature can be introduced onto the rail pad as well to save material and cost of the rail pad.

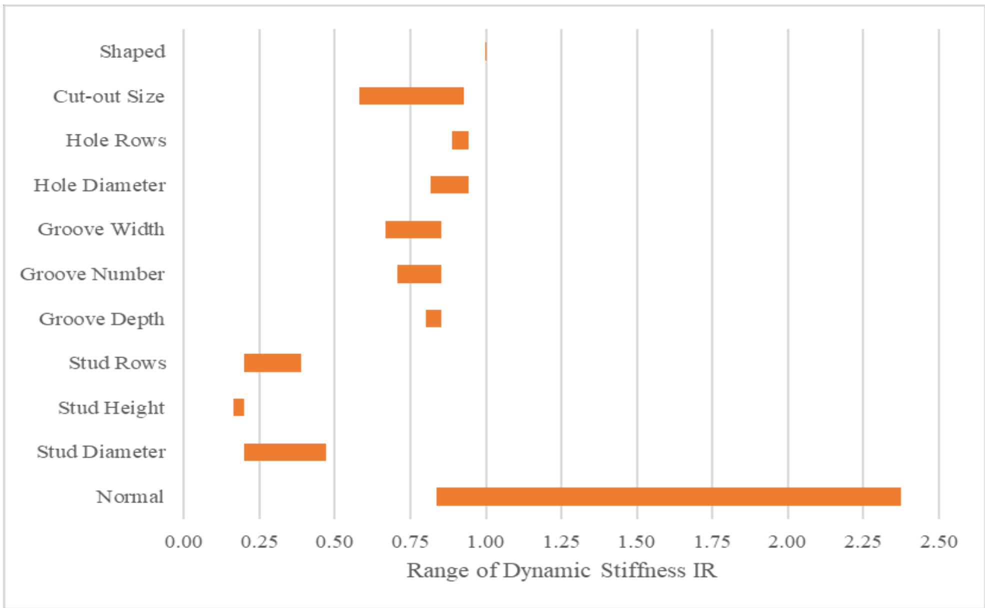

Figure 4.12: Range of IR for Dynamic Stiffness for All Features

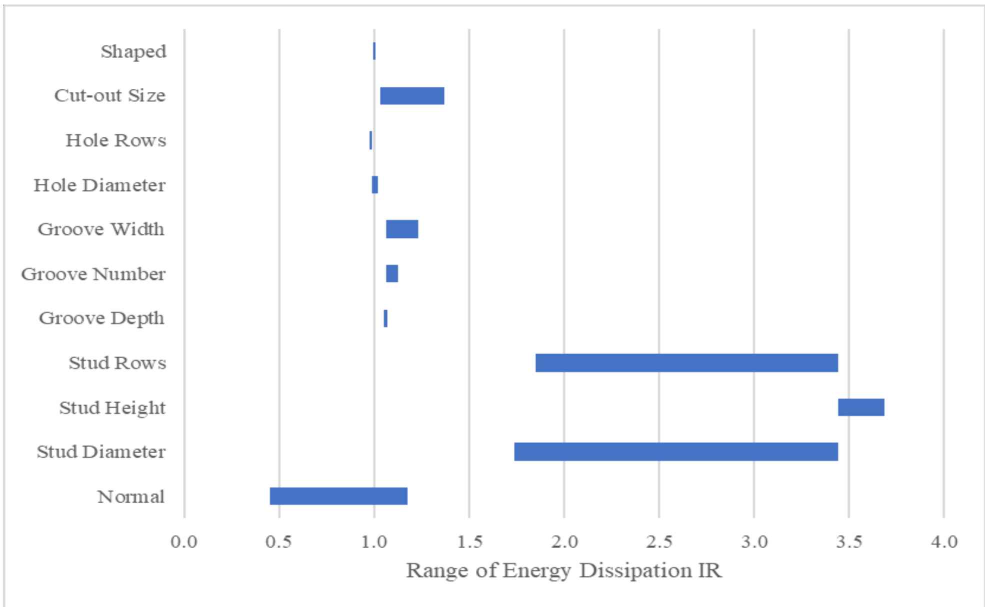

Figure 4.13: Range of IR for Energy Dissipation for All Features

CHAPTER 5

CONCLUSION AND DISCUSSIONS

5.1 Conclusion

This study has investigated the geometrical impact of the normal, studded, grooved, holed, cut-out, and shaped rail pad designs using simulation. For normal rail pad, it was found that the dynamic stiffness decreases and the energy dissipation increases as thickness becomes larger. Moreover, it was also found that the relation between dynamic stiffness and thickness can be well represented by the power law model. These observations agree with the findings from previous studies. However, the power law relation derived in this study indicates that dynamic stiffness is inversely proportional to thickness and contradicts the finding of previous study, which might be due to the material used in the previous study is different. Also, the dynamic properties of normal rail pad vary greatly as thickness changes.

For studded rail pad, it was found that the significant features in influencing dynamic properties are the stud diameter and number of stud rows. Therefore, these features need to be given the most attention while designing the geometry of studded rail pad. Also, the attenuation of dynamic properties with the stud features are limited and cannot fully compensate the lost dynamic stiffness and gained energy dissipation due to the introduction of studs.

For grooved rail pad, groove width produces the largest impact on the dynamic properties among the features, while the groove number considerably alters dynamic stiffness but minorly affects energy dissipation. Hence, groove width and groove number should receive the highest priority in designing grooved rail pad. Furthermore, the addition of grooves only reduces dynamic stiffness and increases energy dissipation, which means grooved rail pad can only have smaller dynamic stiffness and higher energy dissipation than the normal rail pad of equal thickness.

For holed rail pad, hole diameter has more significant effect on the dynamic stiffness than the number of hole rows. Meanwhile, both features barely affect the energy dissipation. This shows that the hole feature mainly adjusts the dynamic stiffness. Moreover, trends of the dynamic stiffness with changing hole dimensions indicate that dynamic stiffness of holed rail pad is always lower than that of no-hole rail pad.

For cut-out rail pad, the size of the cut-out was demonstrated to substantially affect the dynamic properties, making it also a significant feature. When compared with holed design, the cut-out design compromises less on dynamic stiffness for a certain amount of material removed, showing that the cut-out design has more material saving capacity than holed design for the application of rail pad.

For shaped rail pad, it was observed that the dynamic properties variation due to rail pad shape is in a very minor range. This shows that the shape is not a significant factor that needs to be considered for adjusting rail pad dynamic properties.

As an overview, the thickness of rail pad is the only factor that can effectively increase dynamic stiffness and lower energy dissipation. All the proposed designs except normal rail pad are only capable of achieving dynamic stiffness similar to or lower than the baseline design. Similarly, the energy dissipation achievable by all designs except normal rail pad is only similar to or higher than the baseline design. The thickness is the most significant features, followed by the stud feature, and then the cut-out feature. In addition, the introduction of all features except the hole and shape causes a trade-off between dynamic stiffness and energy dissipation where this trade-off is most apparent for the studded design.

5.2 Recommendations for Future Work

There are a few recommendations given for future researches. Since this study does only simulation work, it is recommended to carry out experiments on actual rail pads to complement the result of this study. To do so, the researchers need to have access to FC9 rail pads, which are the rail pads used in this study, and perform compression test with the universal testing machine. The tests should be conducted by setting the same loading conditions and temperature stated in Chapter 3 to obtain the hysteresis curve. The same calculations are then performed again to compute the dynamic stiffness and energy dissipation. With the availability of experimental data, it can then be compared with the simulation results to further validate the findings in this study.

Aside from that, it is also recommended to investigate the effect of different rail pad material on the dynamic properties of the rail pad designs discussed in this study with simulation. It is logical to conduct studies on the dynamic properties of rail pad of different material since there are many different materials available. Examples of the commonly used material for rail pad includes the EPDM and TPE. To conduct such studies, the hyper-elastic and Prony series material data for simulation can be obtained from the uniaxial tensile test and double-shear sweep test respectively as done by Li et al. (2020). The result of the future study can thus be compared with the results of this study, especially the trendline functions. If both studies suggest the same trendline function, it implies that the function is applicable on all rail pad material.

Lastly, it is also recommended to carry out studies on the practical limit of the dimensions of the different rail pad designs. The features and dimensions proposed in this study does not consider the stress developed when loaded. Therefore, the proposed dimensions of the features in this study might be unrealistic for the rail pad to sustain the massive dynamic load; the proposed design might fail or tear during actual operation. More studies are needed to investigate if the dimensions proposed are practical for rail pad application and establish a limit onto the practical dimension of the rail pad features. This kind of study will also involve determining the failure criterion of the rubber material and the necessary parameter for establishing the failure criterion.

REFERENCES

Ali, N. kadum A., M.Farhan, M. and Moosa, A. S. (2017) 'The Effect of Shape Factor on the Operation Periods of Anti-Vibration Rubber', *IISTE*, 17(6), pp. 437–447.

Bhardawaj, S., Sharma, R. C. and Sharma, S. K. (2019) 'A survey of railway track modelling', *International Journal of Vehicle Structures and Systems*, 11(5), pp. 508–518.

Callister, W. D. and Rethwisch, D. G. (2014) *Materials Science and Engineering*. 9th edn, *Wiley*. 9th edn. John Wiley and Sons, Inc.

Chen, J. and Zhou, Y. (2020) 'Dynamic vertical displacement for ballastless track-subgrade system under high-speed train moving loads', *Soil Dynamics and Earthquake Engineering*, 129, p. 105911.

Doshin Rubber. (n.d.) *Base Isolation High Damping Rubber Bearing*. Retrieved from https://doshinrubber.com/high-damping-rubber-bearing/

Egana, J. I., Vinolas, J. and Seco, M. (2006) 'Investigation of the influence of rail pad stiffness on rail corrugation on a transit system', *Wear*, 261(2), pp. 216–224.

Fatima, I. D., Shafi, N. and Anjum, H. (2019) 'Viscoelastic Properties of Rubber Material Modelling', *2019 International Conference on Applied and Engineering Mathematics, ICAEM 2019 - Proceedings*, pp. 117–121.

Grassie, S. L. and Cox, S. J. (1984) 'The Dynamic Response of Railway Track With Flexible Sleepers to High Frequency Vertical Excitation', in *Proceedings of the Institution of Mechanical Engineers Part D Journal of Automobile Engineering*, pp. 117–124.

Habieb, A. B., Valente, M. and Milani, G. (2019) 'Base seismic isolation of a historical masonry church using fiber reinforced elastomeric isolators', *Soil Dynamics and Earthquake Engineering*, 120(September 2018), pp. 127–145.

He, Q., Cai, C., Zhu, S., Zhang, J. and Zhai, W (2018) 'Dynamic performance of low vibration slab track on shared high-speed passenger and freight railway', *Transport*, 33(3), pp. 669–678.

Indraratna, B., Ngo, N. T. and Rujikiatkamjorn, C. (2017) 'Improved Performance of Ballasted Rail Tracks Using Plastics and Rubber Inclusions', *Procedia Engineering*, 189(May), pp. 207–214.

Jin, H., Zhou, S. and Liu, W. (2017) ‘Optimization of vibration reduction of the rubber floating-slab tracks’, *Journal of Vibroengineering*, 19(2), pp. 1214–1224.

Ju, S. H., Kuo, H. H. and Ni, S. H. (2018) ‘Vibration Induced by Moving Cranes in High-Tech Buildings due to Rail Pad Materials’, *Shock and Vibration*, 2018.

Kaewunruen, S. and Remennikov, A. M. (2008) ‘An alternative rail pad tester for measuring dynamic properties of rail pads under large preloads’, *Experimental Mechanics*, 48(1), pp. 55–64.

Kareaga Laka, Z. (2016) *Dynamic Stiffness and Damping Prediction on Rubber Material Parts , FEA and Experimental Correlation*, *London Metropolitan University*. London Metropolitan University. Available at: https://core.ac.uk/download/pdf/76979813.pdf.

Kim, B., Lee, S. B., Lee, J., Cho, S., Park, H., Yeom, S. and Park, S. H. (2012) ‘A comparison among Neo-Hookean model, Mooney-Rivlin model, and Ogden model for Chloroprene rubber’, *International Journal of Precision Engineering and Manufacturing*, 13(5), pp. 759–764.

Li, M., Chen, J., Zhu, R., Duan, C., Wang, S. and Lu, X. (2020) ‘Dynamic stiffness and damping characteristics of a shaft damping ring: A combined hyperelastic and viscoelastic constitutive model’, *Shock and Vibration*, 2020.

Li, Z., Lou, J., Zhu, S. and Tang, S. (2011) ‘Simulation on performance of rubber isolator based on ANSYS’, *2011 2nd International Conference on Mechanic Automation and Control Engineering, MACE 2011 - Proceedings*, (1), pp. 1608–1611.

Mooney, M. (1940) ‘A theory of large elastic deformation’, *Journal of Applied Physics*, 11(9), pp. 582–592.

Oregui, M., De Man, A., Woldekidan, M. F., Li, Z. and Dollevoet, R. (2016) ‘Obtaining railpad properties via dynamic mechanical analysis’, *Journal of Sound and Vibration*, 363, pp. 460–472.

Oregui, M., Nunez, A., Dollevoet, R. and Li, Z. (2017) ‘Sensitivity Analysis of Railpad Parameters on Vertical Railway Track Dynamics’, *Journal of Engineering Mechanics*, 143(5), p. 04017011.

Ouyang, Z., Luo, Y. and Liu, Y. (2015) ‘The Geometry Optimization of Shear-Type Track Rubber Absorber Based on Finite Element Method’, *Proceedings - 2015 7th International Conference on Measuring Technology and Mechatronics Automation, ICMTMA 2015*, pp. 1216–1219.

Rahnavard, R., Craveiro, H. D. and Napolitano, R. (2020) ‘Static and dynamic stability analysis of a steel-rubber isolator with rubber cores’, *Structures*, 26(May), pp. 441–455.

Rivlin, R. S. (1948) 'Large elastic deformations of isotropic materials IV. further developments of the general theory', *Philosophical Transactions of the Royal Society of London. Series A, Mathematical and Physical Sciences*, 241(835), pp. 379–397.

Sainz-Aja, J. A., Carrascal, I. A., Ferreno, D., Pombo, J., Casado, J. A. and Diego, S. (2020) 'Influence of the operational conditions on static and dynamic stiffness of rail pads', *Mechanics of Materials*, 148(December 2019).

Santhosh, S., Velmurugan, V., Paramasivam, V. and Thanikaikarasan, S. (2020) 'Experimental investigation and comparative analysis of rubber engine mount vibration and noise characteristics', *Materials Today: Proceedings*, 21, pp. 638–642.

Shi, G., Wang, K., Huang, Q. and Zhang, X. (2017) 'Influences of stiffness of rail pads on system dynamic performances of heavy haul railway', *Communications in Computer and Information Science*, 762, pp. 618–628.

Sol-Sánchez, M., Moreno-Navarro, F. and Rubio-Gámez, M. C. (2014) 'The use of deconstructed tire rail pads in railroad tracks: Impact of pad thickness', *Materials and Design*, 58, pp. 198–203.

Sol-Sánchez, M., Moreno-Navarro, F. and Rubio-Gámez, M. C. (2015) 'The use of elastic elements in railway tracks: A state of the art review', *Construction and Building Materials*, 75, pp. 293–305.

Wei, K., Liu, Z., Liang, Y. and Wang, P. (2016) 'An investigation into the effect of temperature-dependent stiffness of rail pads on vehicle-track coupled vibrations', *Proceedings of the Institution of Mechanical Engineers, Part F: Journal of Rail and Rapid Transit*, 231(4), pp. 444–454.

Wei, K., Yang, Q., Dou, Y., Wang, F. and Wang, P. (2017) 'Experimental investigation into temperature- and frequency-dependent dynamic properties of high-speed rail pads', *Construction and Building Materials*, 151, pp. 848–858.

Wei, K., Zhang, P. and Wang, P. (2016) 'Influence of amplitude- and frequency-dependent stiffness of rail pads on the frequency-domain random vibration of vehicle-track coupled system', *Shock and Vibration*, 34(4), pp. 108–115.

Wu, J., Liu, C., Jiang, H. and Wang, Z. (2020) 'Numerical modeling and experimental testing analysis of Assembled Rubber Metal Isolator', *Science progress*, 103(3), pp. 1–23.

Xin, T., Ding, Y., Wang, P. and Gao, L. (2020) 'Application of rubber mats in transition zone between two different slab tracks in high-speed railway', *Construction and Building Materials*, 243, pp. 118219.

Xu, L., Liu, H. and Yu, Z. (2022) ‘A coupled model for investigating the interfacial and fatigue damage evolution of slab tracks in vehicle-track interaction’, *Applied Mathematical Modelling*, 101, pp. 772–790.

Yeoh, O. H. (1993) ‘Some forms of the strain energy function for rubber’, *Rubber Chemistry and Technology*, pp. 754–771.

Zakeri, J. A., Fattahi, M., Nouri, M. and Janatabadi, F. (2020) ‘Influence of rail pad stiffness and axle loads on dynamic responses of train-track interaction with unsupported sleepers’, *Periodica Polytechnica Civil Engineering*, 64(2), pp. 524–534.

Zakeri, R., Tafreshi, S. N. M., Dawson, A. R. and Baidya, D. K. (2021) ‘Influence of rubber sheet on dynamic response of machine foundations’, *Construction and Building Materials*, 274, p. 121788.

APPENDICES

Appendix A: Project Management Tool

Appendix A-1: Gantt Chart of the Project

Project Activities		**W1**	**W2**	**W3**	**W4**	**W5**	**W6**	**W7**	**W8**	**W9**	**W10**	**W11**	**W12**	**W13**	**W14**
Simulation of Rail Pad Geometry	Plan														
	Actual														
Effect of Geometry Result Analysis	Plan														
	Actual														
Result Table and Properties Graph Preparation	Plan														
	Actual														
Final Report Writing, Poster Design, and Presentation	Plan														
	Actual														

Appendix B: Graphical Result of the Simulation Study

Appendix B-1: Simulation Result of Normal Rail Pad (10.5 mm)

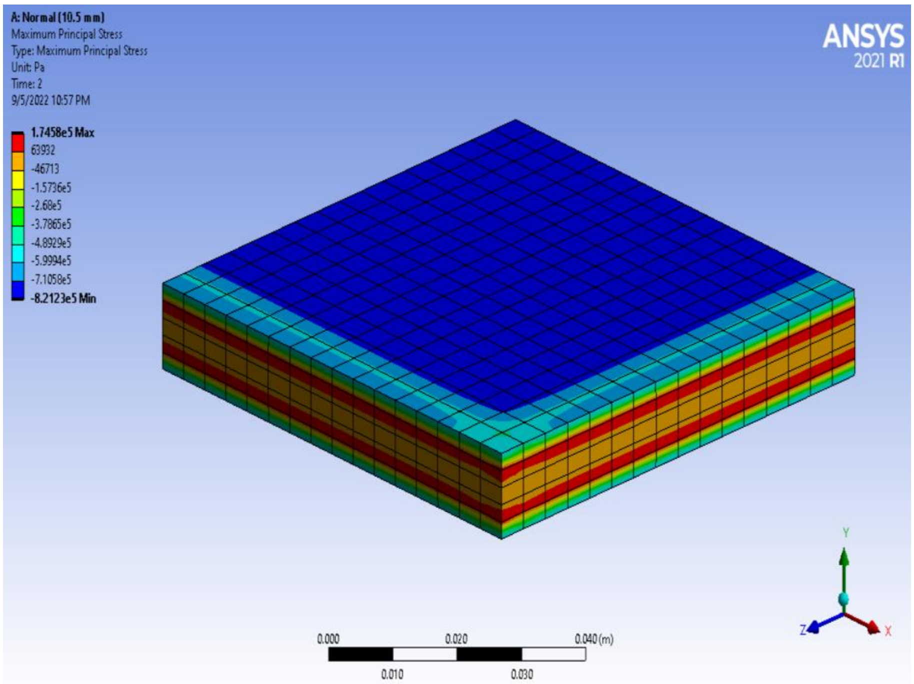

Appendix B-2: Simulation Result of Studded Rail Pad (Basic Design)

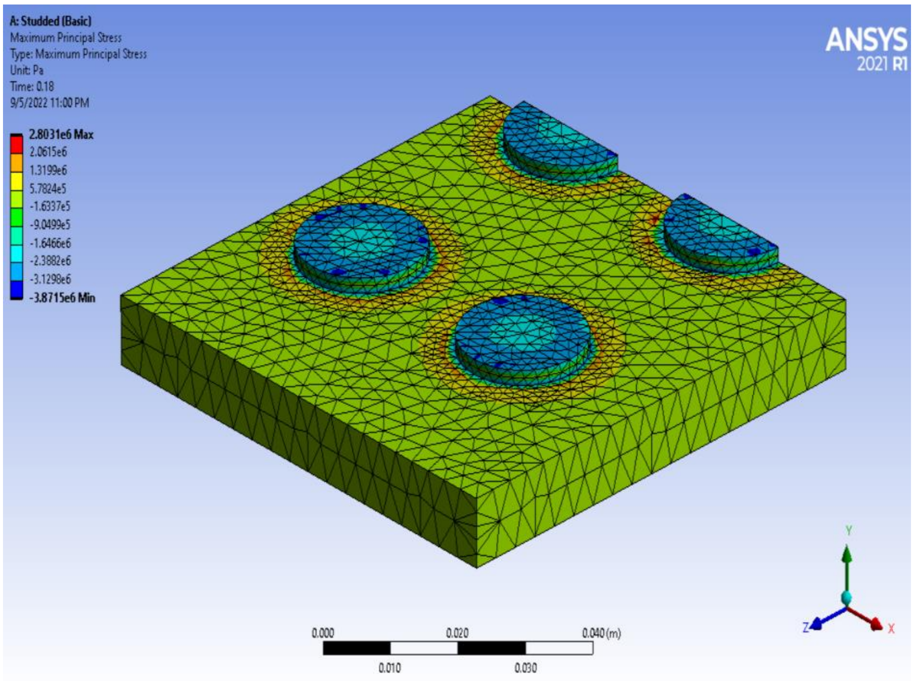

Appendix B-3: Simulation Result of Grooved Rail Pad (Basic Design)

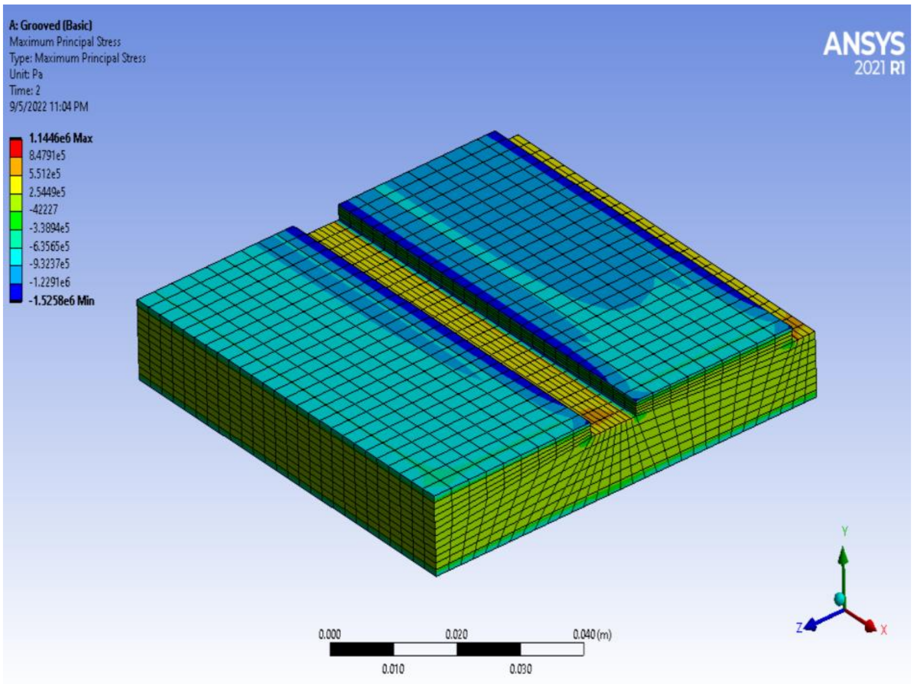

Appendix B-4: Simulation Result of Holed Rail Pad (Basic Design)

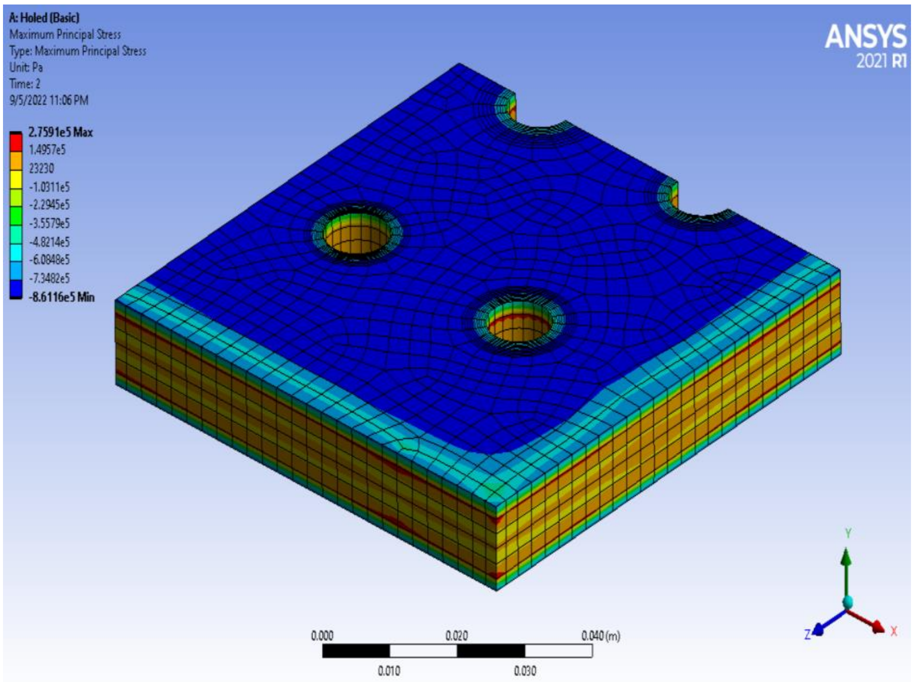

Appendix B-5: Simulation Result of Cut-out Rail Pad (38 mm × 38 mm)

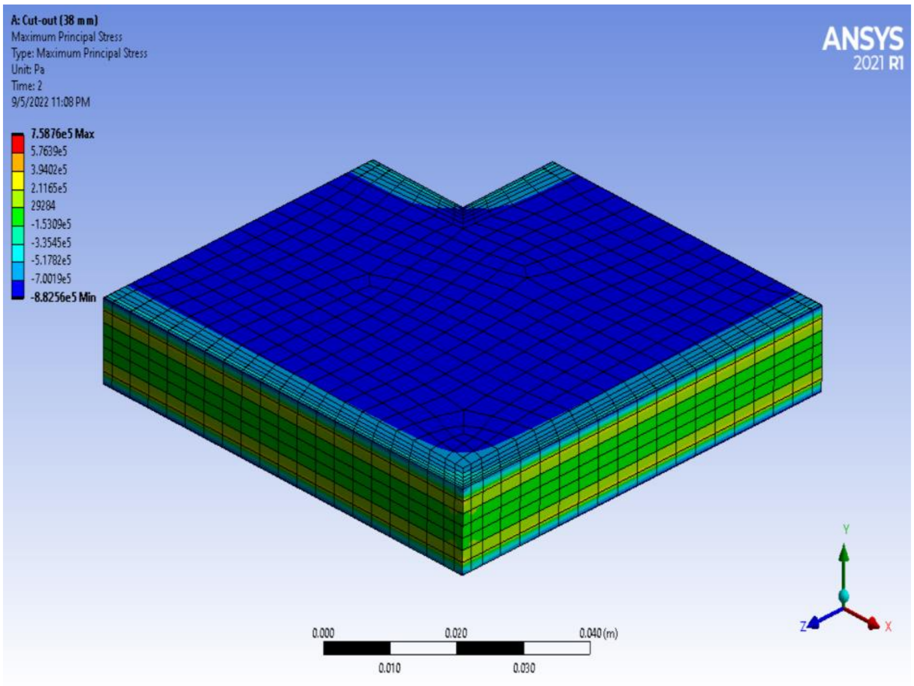

Appendix B-6: Simulation Result of Circle Rail Pad

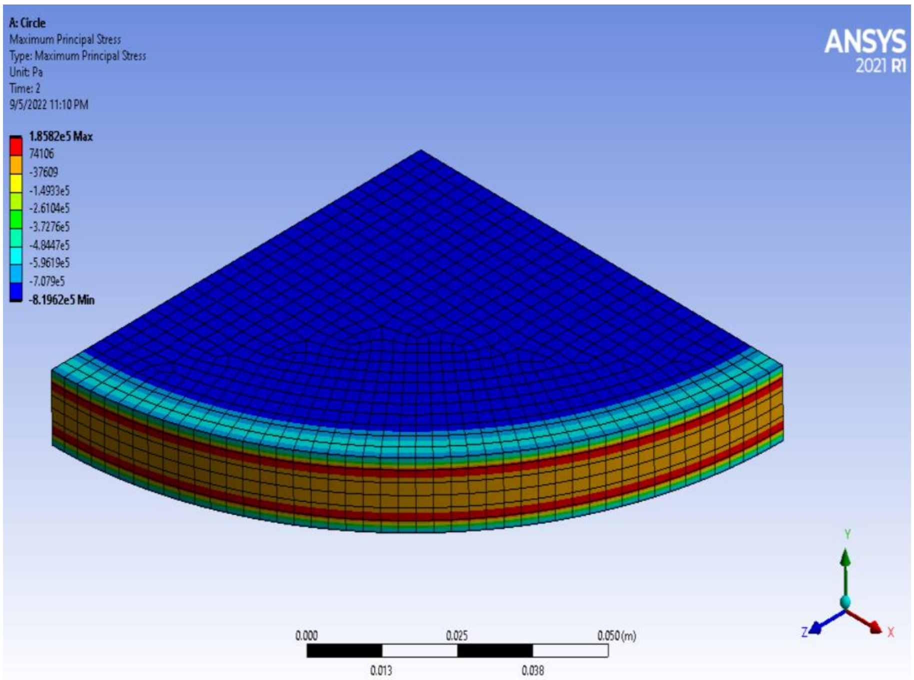

Appendix B-7: Simulation Result of Triangle Rail Pad

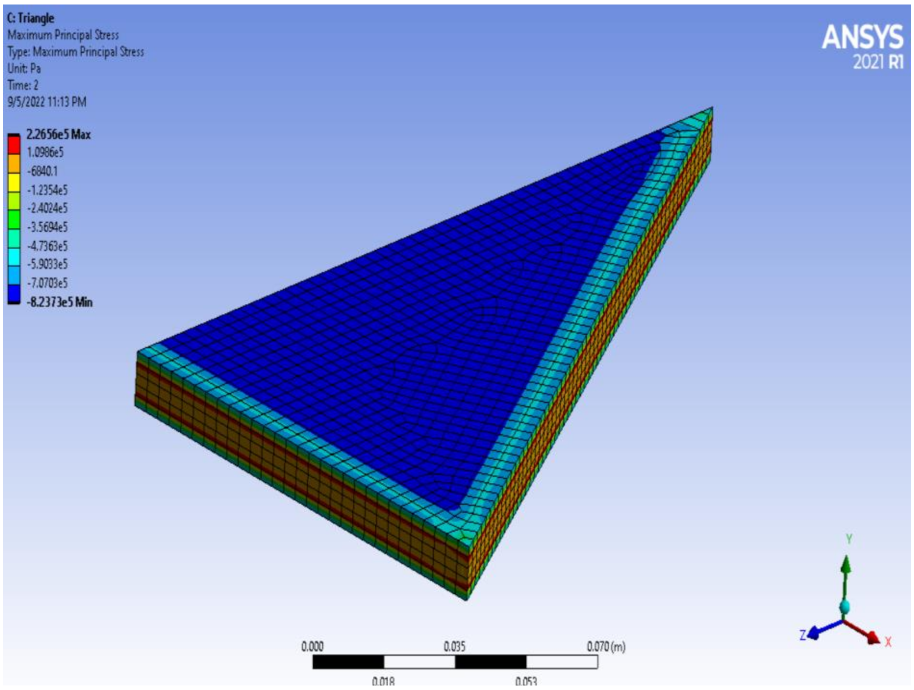

Appendix B-8: Simulation Result of Pentagon Rail Pad

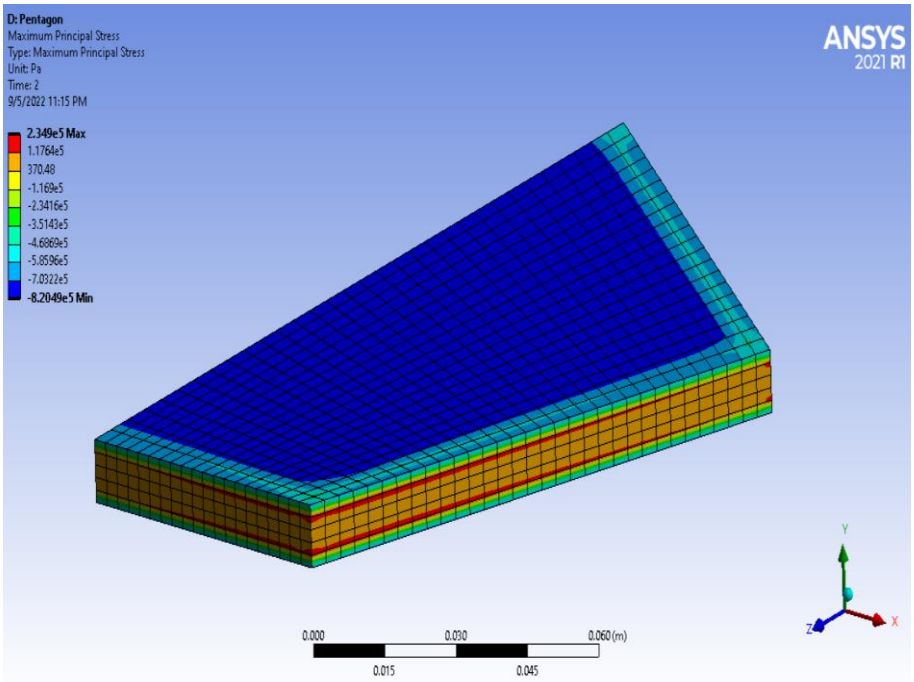

Appendix B-9: Simulation Result of Hexagon Rail Pad

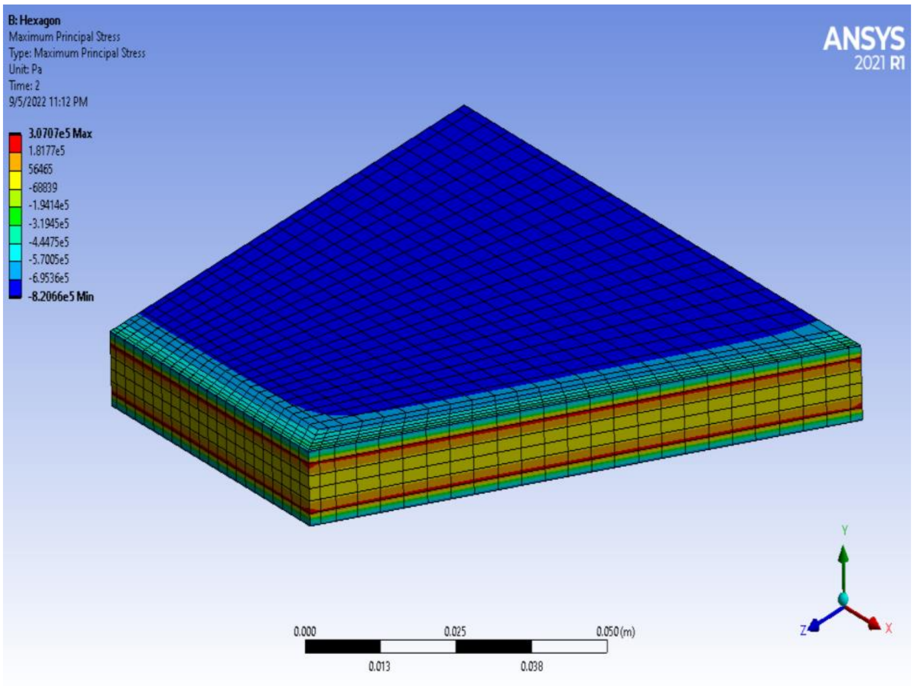

Appendix C: Full Result of the Study

Appendix C-1: Dynamic Stiffness for All Rail Pad Geometry

Normal	4.5	6.5	8.5	10.5	12.5
Stiffness (kN/mm)	1535.96	1056.92	803.32	646.4	539.56

Studded	20	24	28	32	Stud Diameter
Stiffness (kN/mm)	128.184	177.852	236.468	303.492	
	2.0	3.5	5.0	6.5	Stud Height
	128.184	119.972	112.68	106.332	
	3	4	5	6	Stud Rows
	128.184	169.192	210.824	251.884	

Grooved	2.0	3.5	5.0	6.5	Groove Depth
Stiffness (kN/mm)	550.48	538.6	528.12	518.68	
	3	4	5	6	Groove Number
	550.48	519.24	487.64	457.52	
	9	12	15	18	Groove Width
	550.48	509.96	469.92	430.48	

Holed	10	13	16	19	Hole Diameter
Stiffness (kN/mm)	609.36	587	559.76	528.04	
	3	4	5	6	Hole Rows
	609.36	597.32	585.52	574.12	

Cut-out	38	57	76	95	Cut-out Size
Stiffness (kN/mm)	599.2	544.8	469.88	374.78	

Shaped	Triangle	Square	Pentagon	Hexagon	Circle
Stiffness (kN/mm)	643.9	646.4	647.14	646.96	648.08

Appendix C-2: Energy Dissipation for All Rail Pad Geometry

Normal	4.5	6.5	8.5	10.5	12.5
Energy Dissipation (J)	0.09748	0.13884	0.17892	0.2178	0.25528

Studded	20	24	28	32	Stud Diameter
Energy Dissipation (J)	0.74988	0.57504	0.45884	0.37764	
	2.0	3.5	5.0	6.5	Stud Height
	0.74988	0.79468	0.80272	0.77984	
	3	4	5	6	Stud Rows
	0.74988	0.56912	0.4654	0.40268	

Grooved	2.0	3.5	5.0	6.5	Groove Depth
Energy Dissipation (J)	0.23056	0.23192	0.23104	0.22844	
	3	4	5	6	Groove Number
	0.23056	0.2348	0.23936	0.24452	
	9	12	15	18	Groove Width
	0.23056	0.24084	0.25348	0.26852	

Holed	10	13	16	19	Hole Diameter
Energy Dissipation (J)	0.21472	0.21572	0.21784	0.22136	
	3	4	5	6	Hole Rows
	0.21472	0.21372	0.21292	0.21248	

Cut-out	38	57	76	95	Cut-out Size
Energy Dissipation (J)	0.22472	0.23852	0.26164	0.29808	

Shaped	Triangle	Square	Pentagon	Hexagon	Circle
Energy Dissipation (J)	0.2156	0.2178	0.21848	0.21832	0.21916

Appendix C-3: Dynamic Stiffness IR for All Rail Pad Geometry

Normal	4.5	6.5	8.5	10.5	12.5
Stiffness (kN/mm)	2.376	1.635	1.243	1.000	0.835

Studded	20	24	28	32	Stud Diameter
Stiffness (kN/mm)	0.198	0.275	0.366	0.470	
	2.0	3.5	5.0	6.5	Stud Height
	0.198	0.186	0.174	0.164	
	3	4	5	6	Stud Rows
	0.198	0.262	0.326	0.390	

Grooved	2.0	3.5	5.0	6.5	Groove Depth
Stiffness (kN/mm)	0.852	0.833	0.817	0.802	
	3	4	5	6	Groove Number
	0.852	0.803	0.754	0.708	
	9	12	15	18	Groove Width
	0.852	0.789	0.727	0.666	

Holed	10	13	16	19	Hole Diameter
Stiffness (kN/mm)	0.943	0.908	0.866	0.817	
	3	4	5	6	Hole Rows
	0.943	0.924	0.906	0.888	

Cut-out	38	57	76	95	Cut-out Size
Stiffness (kN/mm)	0.927	0.843	0.727	0.580	

Shaped	Triangle	Square	Pentagon	Hexagon	Circle
Stiffness (kN/mm)	0.996	1.000	1.001	1.001	1.003

Appendix C-4: Energy Dissipation IR for All Rail Pad Geometry

Normal	4.5	6.5	8.5	10.5	12.5
Energy Dissipation (J)	0.448	0.637	0.821	1.000	1.172

Studded	20	24	28	32	Stud Diameter
Energy Dissipation (J)	3.443	2.640	2.107	1.734	
	2.0	3.5	5.0	6.5	Stud Height
	3.443	3.649	3.686	3.581	
	3	4	5	6	Stud Rows
	3.443	2.613	2.137	1.849	

Grooved	2.0	3.5	5.0	6.5	Groove Depth
Energy Dissipation (J)	1.059	1.065	1.061	1.049	
	3	4	5	6	Number of Grooves
	1.059	1.078	1.099	1.123	
	9	12	15	18	Groove Width
	1.059	1.106	1.164	1.233	

Holed	10	13	16	19	Hole Diameter
Energy Dissipation (J)	0.986	0.990	1.000	1.016	
	3	4	5	6	Hole Rows
	0.986	0.981	0.978	0.976	

Cut-out	38	57	76	95	Cut-out Size
Energy Dissipation (J)	1.032	1.095	1.201	1.369	

Shaped	Triangle	Square	Pentagon	Hexagon	Circle
Energy Dissipation (J)	0.990	1.000	1.003	1.002	1.006